Revista Mexicana de Astronomía y Astrofísica, **48**, 109–136 (2012)

uvby-β PHOTOMETRY AND KINEMATICS OF METAL-POOR STARS: A SEARCH FOR MOVING GROUPS IN THE GALACTIC STELLAR HALO

J. S. Silva,[1,2] W. J. Schuster,[1] and M. E. Contreras[1]

Received 2011 October 20; accepted 2012 January 10

RESUMEN

Se ha examinado la posible presencia de grupos en movimiento en el Halo galáctico en base a la nueva fotometría $uvby-\beta$ de 143 estrellas pobres en metales, unida a la fotometría de las 1533 estrellas de los catálogos previos de Schuster & Nissen (1988), Schuster et al. (1993) y Schuster et al. (2006). Este nuevo conjunto de datos fotométricos junto con la velocidad radial y los movimientos propios tomados de la literatura permitió obtener las componentes de velocidad galáctica U', V', y W' para casi toda la muestra. Con esta información cinemática se obtuvieron tres diagramas: [Fe/H] vs $V_{\rm rot}$, Bottlinger (V' vs U') y Toomre (V' vs $(U'^2 + W'^2)^{1/2}$), usados para identificar grupos de estrellas comunes a cada uno de ellos. Una vez identificados, se compararon con grupos en movimiento reportados en la literatura. En particular, se identificaron posibles miembros de los grupos Kapteyn y ω Cen.

ABSTRACT

The possible presence of moving groups in the local Galactic stellar halo has been examined based on new $uvby-\beta$ photometry for a sample of 143 metal-poor stars joined to the photometry of 1553 stars from the previous catalogues of Schuster & Nissen (1988), Schuster et al. (1993), and Schuster et al. (2006). This new set of photometric data, together with radial velocities and proper motions taken from the literature, have allowed us to obtain Galactic space velocities U', V', and W' for nearly the entire sample. With this kinematic information, three diagrams: the [Fe/H] vs $V_{\rm rot}$, the Bottlinger (V' vs U') and the Toomre (V' vs $(U'^2+W'^2)^{1/2}$) have been obtained and used to identify probable groups of stars in common between them. Once identified, these groups were compared to moving groups reported in the literature. In particular, probable members of the Kapteyn group and ω Cen were identified.

Key Words: Galaxy: halo — Galaxy: kinematics and dynamics — Galaxy: structure — stars: kinematics and dynamics — stars: Population II — techniques: photometric

© Copyright 2012: Instituto de Astronomía, Universidad Nacional Autónoma de México

1. INTRODUCTION

Since the early work of Eggen, Lynden-Bell, & Sandage (1962, hereafter ELS), the history and formation of our Galaxy and its halo has been a fundamental topic in astronomy. ELS proposed a monolithic collapse model of the Milky Way which was widely accepted until some observational data pointed to the idea of a rather hierarchical galaxy formation model. The main study that challenged the ELS interpretation was that of Searle & Zinn (1978, hereafter SZ). The globular cluster system, studied by SZ as a tracer of the stellar halo kinematic properties, seems to be consistent with a formation process in which smaller subunits were aggregated in a hierarchical way. Nowadays, the Milky Way formation scenario seems to be a combination of both models (Freeman & Bland-Hawthorn 2002). While the formation of the spheroidal component takes into account the basic ideas of ELS plus SZ, the disk is the result of a smooth and gradual process. However, although the disk is believed to be formed in a quiescent way it is not considered as a stationary structure. It evolves as the result of both internal

[1]Instituto de Astronomía, Universidad Nacional Autónoma de México, Mexico.
[2]Observatório Nacional/MCT, Rio de Janeiro, Brazil.

© Copyright 2012: Instituto de Astronomía, Universidad Nacional Autónoma de México

and external interactions. Internal inhomogeneities, such as spiral arms and molecular clouds, and external mergers with satellite galaxies cause perturbations on the disk that force it to change in time. In fact, the presence of two substructures in the disk (the thin and the thick disk) is widely accepted as the result of the dynamical heating of an early thin disk by a satellite roughly 10 Gyr ago (Quinn & Goodman 1986; Wyse et al. 2006, and various others).

The close interaction of our Galaxy with satellite galaxies in the past is now being related also to some of the groups of stars in the solar neighborhood, sharing kinematic characteristics and identified since the pioneering works of Proctor (1869), Kapteyn (1905), Hertzsprung (1909) and Lindblad (1925). After these studies, O.J. Eggen established, in a series of papers, the spatial and kinematic properties of what he called 'stellar streams' (Eggen 1958, 1977, 1996b,c). Throughout his works, Eggen identified several of these streams of stars and actually defined two kinds of associations, 'superclusters' and 'stellar moving groups' (Eggen 1994). He defined a supercluster as a group of stars dispersing from a cluster and sharing kinematic features, and a 'stellar moving group', as a group of stars, belonging to a completely disrupted supercluster whose original orbit was replaced by a tube of orbits that enters our solar neighbourhood and shows a small range in velocity along the tube. At present, it seems that moving groups could have different origins. One may be related to that suggested by Eggen, dispersion of stellar clusters, but other moving groups may be the result of dynamic or resonant mechanisms within the Galaxy (Mayor 1972; Kalnajs 1991; Dehnen 1998; Skuljan, Hearnshaw, & Cottrell 1999; Fux 2001; Antoja et al. 2009, 2010). Finally, there is a third possible scenario that relates moving groups to the debris of accreted and disrupted dwarf galaxies (Navarro, Helmi, & Freeman 2004; Helmi et al. 2006).

On one hand, many works have been dedicated to the study of the classical young moving groups in the solar neighbourhood, mainly concentrated in the galactic disk, such as the Hyades supercluster (Eggen 1958, 1960a, 1984, 1992b, 1996a, 1998a; Montes et al. 2001), the Ursa Majoris Group (Sirius Supercluster; Eggen 1960b, 1983a, 1992c, 1998b; Soderblom & Mayor 1993a,b; Montes et al. 2001), the so-called Local Association (Pleiades moving group; Eggen 1975, 1983c,d, 1992a, 1995a; Montes et al. 2001), IC 2391 (Eggen 1991, 1995b; Montes et al. 2001), Castor Moving Group (Barrado y Navascués 1998; Montes et al. 2001) and Hercules Group (Dehnen 2000; Fux 2001). In particular, Hipparcos and Tycho-2 Catalogues have been fundamental databases for most of the observational studies that led to the firm establishment of the presence of these moving groups in the solar neighbourhood and moreover, the discovery of substructures within them (Chereul, Crézé, & Bienaymé 1998; Asiain et al. 1999; Skuljan et al. 1999; Famaey et al. 2005; Antoja et al. 2008). Theoretically, some of the young moving groups have been used to test the hypothesis that galactic bar resonances can produce kinematical groups in the galactic disk (Kalnajs 1991) and also that the spiral arms can affect the velocity distribution (Antoja et al. 2010, 2011; Famaey, Siebert, & Minchev 2011). The Geneva-Copenhagen survey of nearby F- and G-type dwarf stars (Nordström et al. 2004) has produced metallicities, ages, kinematics, and Galactic orbits for nearly 17,000 stars, and their Bottlinger diagram shows considerable structure, but for groups of stars which are not coeval; they conclude that these structures are most likely produced by the dynamical effects of the non-axisymmetric Galactic components, such as the spiral arms or the Galactic bar.

On the other hand, large surveys have been employed to look for structure in the Galactic Halo like the dedicated spaghetti survey (Morrison et al. 2000; Starkenbug et al. 2009, and references therein), or much more widespread galactic and stellar surveys, used by some authors for the same purpose, like the Sloan Digital Sky Survey and Extension, SDSS and SEGUE, respectively (Klement et al. 2009; Correnti et al. 2010, and references therein). RR Lyrae variable-star surveys, QUEST, (Zinn et al. 2004; Vivas et al. 2008) and SEKBO (Prior, Da Costa, & Keller 2009; Keller, Da Costa, & Prior 2009, and references therein) have also produced interesting and useful results. In addition, red and very-red giants have been traced very successfully to study halo substructure using the 2MASS infrared survey by Rocha-Pinto et al. (2003) and Sharma et al. (2010), and also a special Washington/DDO51 four-filter technique by Majewski et al. (2000) and Muñoz et al. (2006), and references therein.

Although Eggen's work was mainly concentrated on the study of Disk Population stars, he identified three kinematic stellar groups belonging to the Galactic Halo, namely *Ross 451*, *Groombridge 1830*, and *Kapteyn* (Eggen 1958, 1977, 1990, 1996b,c; Eggen & Sandage 1959). In particular, Eggen's Kapteyn and Arcturus (associated to the Galactic thick disk) groups have been well studied looking for more evidence in favor of one of the possible scenarios described above. In fact, Schuster et al. (2006) have found a thick-disk group with [Fe/H] ~ -0.7,

© Copyright 2012: Instituto de Astronomía, Universidad Nacional Autónoma de México

$X \sim -10.0$, age ∼12.5 Gyr, and $V_{\rm rot} \sim 120$ km s^{-1}, which probably corresponds to the "Arcturus" group as described by Eggen (1971, 1983b), and Navarro et al. (2004). As well, the ω Cen group has been the central object of various studies, since the globular cluster to which it is related has been frequently proposed to be the nucleus of a dwarf galaxy disrupted by our Galaxy's tidal field (Abadi et al. 2003a,b; Bekki & Freeman 2003; Meza et al. 2005; Wylie-de Boer, Freeman, & Williams 2010).

In this work, we present new $uvby-\beta$ photometry and kinematics for 143 metal-poor stars and search for probable moving groups, identified through their kinematic and metallicity distributions. Our observations and data reductions are described in § 2. This new sample together with stars from previous catalogues (Schuster & Nissen 1988; Schuster, Parrao, & Contreras 1993; Schuster et al. 2006) give a total of 1637 stars with photometric indices and Galactic velocities (U', V', W'), presented in § 3. In § 4, three different kinematic diagrams, namely, the [Fe/H] vs $V_{\rm rot}$, the Bottlinger (V' vs U'), and the Toomre (V' vs $(U'^2 + W'^2)^{1/2}$) diagrams are analyzed. On each diagram, number density contours were overplotted in order to identify possible groups of stars sharing similar kinematical and/or metallicity characteristics. In § 5, these group candidates were cross-checked in order to look for stars in common. In this way, we have obtained a list of moving-group candidates composed by stars present in all three diagrams. Then, in § 6, we compare our moving-group candidates with those found in the literature and discuss possible relations with them. Finally, we present our conclusions and possible future work in § 7.

2. OBSERVATIONS AND DATA REDUCTION

The $uvby-\beta$ photometric data were taken using the H. L. Johnson 1.5 m telescope at the San Pedro Mártir Observatory (hereafter OAN-SPM)[3] and the six-channel $uvby-\beta$ Danish photometer described in detail by Schuster & Nissen (1988). Observations were made during eight observing runs: April and October 2004, October 2006, January, June and November 2007, and April, and August/September 2008. Since the four-channel $uvby-\beta$ section of the instrument is really a spectrograph-photometer, the grating angle was calibrated using a cadmium lamp to position the spectra on the exit slots to within about ±1 Å at the beginning of each observing run. Whenever possible, an extinction-star pair near the celestial equator was observed over an air-mass range of $X \geq 0.8$. Spaced throughout each night several "drift" stars were observed symmetrically with respect to the local meridian (two hours east and then two hours west) to measure temporal changes in the photometer. Program stars were observed to at least 50,000 counts in all four channels of $uvby$ and to at least 30,000 counts for the two channels centered at Hβ. For all program stars, the sky background was measured until its contributing error was equal to or smaller than the error in the stellar count.

All data reductions were carried out following the precepts of Grønbech, Olsen, & Strömgren (1976) using computer programs kindly loaned by T. Andersen. Standard stars were selected from the Olsen (1983, 1984) catalogues. The reduction programs create a single instrumental photometric system for each observing run, including nightly atmospheric extinctions and night corrections with linear time dependences. Then, transformation equations from the instrumental to the standard systems of V, $b-y$, m_1, c_1, and β are obtained using all standard stars during that observing period. The equations for the transformation to the standard $uvby-\beta$ system are the linear ones of Crawford & Barnes (1970) and Crawford & Mander (1966).

The final standard $uvby-\beta$ photometry for our program stars is given in two groups: 72 low-metallicity stars (hereafter LM) selected from various spectroscopic and photometric studies in the literature to have [Fe/H] $\lesssim -2.0$ (Table 1); and 71 metal-poor subgiant-star candidates (hereafter SG) provided by B. W. Carney (Table 2). For comparison purposes, 73 solar twins from Meléndez et al. (2010), observed during some of the same observing periods, have also been included in our analyses and figures. A brief description of columns in Tables 1 and 2 is the following:

Column 1: identification name of the star; in cases where only a hyphenated number appears, it corresponds to the Luyten-Palomar Survey (LP numbers).

Columns 2, 3, 4, 5: the V magnitude, and the indices $(b-y)$, m_1, and c_1, respectively.

Columns 6, 7: total number of independent observations for the magnitude V and for the indices $(b-y)$, m_1, and c_1, respectively; for a few stars $N_V < N_u$ due to less than photometric conditions on a few nights of observation; we have shown in previous publications that good values can be obtained for the Strömgren colors and indices (but not for magnitudes), when observing through light cir-

[3]The Observatorio Astronómico Nacional at San Pedro Mártir (OAN-SPM) is operated by the Instituto de Astronomía of the Universidad Nacional Autónoma de México.

TABLE 1

STANDARD PHOTOMETRIC INDICES FOR OUR 72 METAL-POOR STARS

ID	V [mag]	$(b-y)$ [mag]	m_1 [mag]	c_1 [mag]	N_V	N_u	β [mag]	N_β
−13 : 3442	10.290	0.309	0.050	0.387	6	6	2.621	6
−22 : 1833	11.186	0.526	0.329	0.169	7	8	2.521	8
−23 : 12296	10.867	0.372	0.054	0.265	7	7	2.597	7
430-051	12.778	0.370	0.074	0.179	5	5	2.574	6
440-071	13.315	0.414	0.068	0.128	5	5	2.566	5
469-098	12.566	0.447	0.056	0.169	5	5	2.555	5
487-027	12.585	0.333	0.052	0.253	5	5	2.595	5
492-053	12.681	0.343	0.044	0.219	6	6	2.586	5
528-161	12.690	0.439	0.040	0.135	2	2	2.581	2
558-002	12.699	0.327	0.053	0.299	5	5	2.610	5
636-003	12.812	0.377	0.062	0.200	3	3	2.581	3
666-038	13.023	0.435	0.112	0.170	5	5	2.557	5
732-048	12.533	0.316	0.058	0.288	6	6	2.630	5
736-002	12.372	0.322	0.054	0.357	5	5	2.615	5
760-071	13.414	0.376	0.056	0.235	2	2	2.585	2
787-042	12.191	0.420	0.087	0.145	5	5	2.540	5
802-051	11.388	0.407	0.053	0.178	5	6	2.561	6
833-020	12.916	0.454	0.122	0.054	5	5	2.560	5
G14-32	8.374	0.596	0.320	0.371	6	6	2.540	6
G15-10	12.036	0.479	0.058	0.130	4	4	2.530	4
G17-25	9.612	0.474	0.204	0.163	11	11	2.536	7
G17-37	13.495	0.562	0.134	0.169	5	5	2.547	4
G18-21	13.146	0.445	0.039	0.102	4	4	2.543	4
G18-40	12.460	0.399	0.053	0.174	6	6	2.569	6
G19-25	11.703	0.497	0.179	0.130	7	7	2.530	7
G25-24	11.627	0.378	0.054	0.182	5	5	2.575	6
G26-12	12.162	0.349	0.037	0.255	5	5	2.568	5
G26-42	12.531	0.381	0.061	0.223	5	5	2.573	4
G28-31	12.615	0.399	0.039	0.220	5	5	2.588	5
G28-34	12.976	0.621	0.406	0.181	5	5	2.509	5
G28-48	11.089	0.499	0.367	0.232	6	7	2.541	7
G29-23	10.229	0.341	0.058	0.326	5	5	2.586	5
G30-52	8.501	0.496	0.249	0.262	2	2	2.569	2
G43-05	12.442	0.437	0.079	0.105	6	6	2.523	6
G44-38	13.466	0.639	0.335	0.120	4	4	2.489	4
G58-15	13.072	0.437	0.068	0.125	9	9	2.548	9
G65-33	12.907	0.627	0.446	0.158	4	4	2.496	4
G72-34	12.964	0.564	0.228	0.168	3	3	2.515	3
G92-49	12.264	0.681	0.102	0.319	5	5	2.571	5
G94-66	13.876	0.577	0.161	0.117	3	3	2.535	3
G114-42	12.779	0.392	0.114	0.205	7	7	2.570	7
G116-69	12.787	0.474	0.138	0.130	4	4	2.540	4
G117-64	13.013	0.383	0.052	0.177	6	6	2.578	6
G122-43	12.000	0.400	0.054	0.162	5	5	2.584	5
G126-02	11.132	0.670	0.470	0.142	5	5	2.492	5
G126-52	10.993	0.323	0.044	0.344	4	4	2.608	4
G126-62	9.479	0.331	0.064	0.327	6	6	2.589	8
G130-41	13.197	0.557	0.210	0.133	2	2	2.526	2
G137-86	13.132	0.333	0.085	0.264	4	4	2.582	4
G139-16	12.549	0.497	0.048	0.166	4	4	2.555	4
G144-28	12.931	0.457	0.056	0.134	2	2	2.563	2
G149-96	13.665	0.490	0.265	0.070	5	5	2.522	5
G157-38	12.573	0.356	0.054	0.163	1	2	2.607	2
G159-48	12.168	0.357	0.046	0.240	2	2	2.603	2
G165-39	10.067	0.312	0.054	0.364	4	5	2.602	7
G167-50	13.542	0.482	0.115	0.124	5	5	2.528	5
G171-15	11.551	0.455	0.074	0.094	5	5	2.535	5
G171-50	13.073	0.378	0.041	0.179	3	3	2.568	3
G176-27	11.267	0.508	0.344	0.217	5	5	2.533	5
G178-41	12.644	0.372	0.056	0.179	5	5	2.573	5
G188-20	12.646	0.408	0.038	0.276	2	2	2.628	2
G190-15	11.024	0.485	0.055	0.084	6	6	2.543	6
G195-35	13.099	0.486	0.067	0.109	5	5	2.536	5
G199-66	12.672	0.375	0.065	0.175	5	5	2.590	5
G214-01	12.063	0.434	0.062	0.128	3	3	2.545	3
G214-05	11.541	0.394	0.051	0.149	5	5	2.564	5
G267-06	10.825	0.334	0.071	0.242	2	2	2.606	2
HD101063	9.443	0.496	0.151	0.279	6	6	2.548	3
HD205650	9.058	0.373	0.096	0.233	5	5	2.574	4
Wolf 436	12.356	0.375	0.057	0.211	4	4	2.568	4
Wolf 1143	10.989	0.477	0.120	0.118	2	2	2.542	2
GCRV 6728	12.584	0.429	0.099	0.124	2	2	2.566	2

© Copyright 2012: Instituto de Astronomía, Universidad Nacional Autónoma de México

TABLE 2

STANDARD PHOTOMETRIC INDICES FOR OUR 71 METAL-POOR SUBGIANT STARS

ID	V [mag]	$(b-y)$ [mag]	m_1 [mag]	c_1 [mag]	N_V	N_u	β [mag]	N_β
−01 : 1792	9.234	0.524	0.208	0.283	5	6	2.544	6
−18 : 6261	10.825	0.396	0.140	0.289	9	10	2.577	10
+37 : 1458	8.916	0.439	0.058	0.236	11	13	2.554	13
405-060	11.294	0.513	0.058	0.294	13	15	2.575	15
412-048	12.052	0.595	0.161	0.411	11	12	2.599	12
500-093	12.189	0.475	0.091	0.226	11	12	2.541	12
615-196	11.454	0.451	0.153	0.249	9	10	2.555	10
625-044	11.890	0.500	0.070	0.196	5	5	2.580	5
628-018	11.621	0.565	0.146	0.321	7	8	2.582	8
685-044	11.810	0.476	0.031	0.312	5	5	2.606	5
685-047	12.522	0.574	−0.021	0.371	4	4	2.601	4
685-053	12.236	0.528	0.090	0.283	8	9	2.573	9
685-055	11.531	0.532	0.120	0.277	3	3	2.587	3
752-017	11.830	0.427	0.011	0.357	5	5	2.597	5
752-018	11.434	0.484	0.137	0.225	8	8	2.579	8
753-029	11.670	0.518	0.027	0.269	6	8	2.552	8
813-013	12.424	0.486	0.007	0.295	9	9	2.601	9
814-012	12.576	0.453	−0.011	0.342	6	7	2.609	7
814-014	11.637	0.492	0.047	0.331	8	9	2.595	9
830-004	11.525	0.388	0.112	0.301	10	11	2.575	11
867-011	11.897	0.590	0.119	0.293	7	7	2.578	7
G01-30	12.181	0.403	0.035	0.281	12	13	2.602	13
G101-34	10.743	0.511	0.114	0.263	5	6	2.548	6
G102-27	9.049	0.442	0.147	0.349	12	14	2.577	14
G102-47	10.310	0.465	0.088	0.231	9	10	2.550	10
G107-43	10.274	0.425	0.148	0.316	9	11	2.570	11
G107-50	11.642	0.371	0.042	0.334	5	6	2.603	6
G113-22	9.695	0.405	0.110	0.262	5	6	2.564	6
G122-57	8.372	0.539	0.273	0.296	12	13	2.543	13
G128-58	12.080	0.437	0.059	0.312	9	10	2.596	10
G141-19	10.570	0.513	0.008	0.226	5	6	2.550	6
G143-23	12.174	0.400	0.064	0.288	4	4	2.599	4
G146-76	10.485	0.477	0.080	0.292	9	9	2.539	9
G152-67	12.293	0.510	0.006	0.291	7	7	2.589	7
G153-64	11.414	0.486	0.102	0.241	6	7	2.574	7
G154-21	9.682	0.486	0.044	0.277	3	4	2.563	4
G154-25	12.948	0.551	0.009	0.308	6	6	2.596	6
G16-13	9.951	0.399	0.115	0.281	8	8	2.570	8
G16-20	10.815	0.437	0.064	0.286	6	7	2.567	7
G16-28	12.062	0.480	0.130	0.260	6	6	2.562	6
G16-08	11.626	0.494	0.121	0.248	7	7	2.571	7
G161-73	10.834	0.380	0.074	0.321	4	5	2.579	5
G170-47	8.946	0.473	0.041	0.264	3	4	2.528	4
G172-16	10.964	0.422	0.076	0.293	14	16	2.584	16
G179-22	10.674	0.477	0.145	0.258	9	10	2.538	10
G19-27	8.152	0.424	0.163	0.292	3	4	2.559	4
G193-33	8.800	0.384	0.144	0.317	8	9	2.592	9
G196-48	10.345	0.388	0.065	0.279	13	15	2.570	15
G205-42	9.970	0.440	0.075	0.239	6	6	2.544	6
G23-14	10.747	0.522	0.095	0.244	4	5	2.553	5
G23-20	11.568	0.464	0.065	0.257	5	6	2.567	6
G24-25	10.570	0.416	0.109	0.180	5	5	2.573	5
G29-20	9.194	0.497	0.171	0.266	5	6	2.550	6
G33-09	10.583	0.422	0.089	0.277	14	16	2.573	16
G59-18	10.168	0.476	0.152	0.264	9	10	2.547	10
G60-26	9.799	0.441	0.122	0.242	11	12	2.554	12
G80-28	9.975	0.393	0.034	0.285	10	11	2.580	11
G83-45	13.438	0.564	0.037	0.135	6	6	2.566	6
G87-27	9.826	0.504	0.288	0.269	5	6	2.548	6
G09-47	7.686	0.521	0.181	0.398	8	9	2.549	9
G90-03	10.398	0.382	0.038	0.311	5	6	2.576	6
G95-11	11.928	0.460	0.023	0.366	11	13	2.599	13
HD132475	8.564	0.391	0.074	0.292	7	7	2.570	7
HD140283	7.208	0.378	0.035	0.288	9	10	2.557	10
HD148211	7.701	0.364	0.132	0.316	7	9	2.583	9
HD189558	7.737	0.389	0.102	0.293	10	11	2.572	11
HD195137	9.875	0.434	0.114	0.311	2	3	2.586	3
HD210295	9.575	0.580	0.184	0.366	9	10	2.540	10
HD24341	7.878	0.442	0.178	0.286	14	16	2.565	16
LTT6194	12.816	0.413	0.026	0.414	4	4	2.618	4
Ross 740	12.750	0.549	−0.036	0.261	3	3	2.591	3

© Copyright 2012: Instituto de Astronomía, Universidad Nacional Autónoma de México

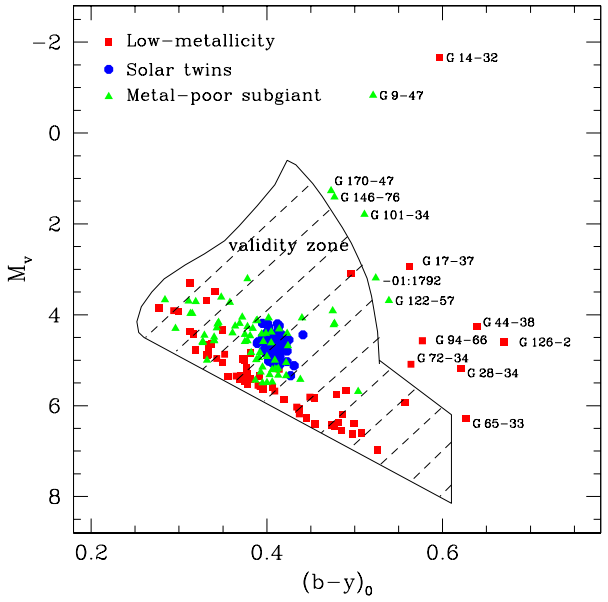

Fig. 1. The M_V versus $(b-y)_0$ diagram showing the region of validity for the photometric absolute-magnitude calibration of our second method described in § 3.1 (Schuster et al. 2004, 2006). The metal-poor stars are shown by (red) squares, the subgiants by (green) triangles, and the solar twins by (blue) circles. Those stars labeled with their names do not fall in the range of validity of this calibration, and are discussed in the text.

rus clouds with the simultaneous 6-channel $uvby-\beta$ photometer at OAN-SPM.

Column 8: the β value on the standard system.

Column 9: total number of independent observations for β.

3. PHOTOMETRIC AND KINEMATIC PARAMETERS

3.1. *Distance determination*

For the photometric distance determination it is necessary to obtain the absolute magnitude, M_V, for each star in these samples. Two methods have been consulted, but mainly the M_V's and distances have been taken from the second one mentioned below. The first method uses an absolute magnitude calibration for late F and G dwarfs and subgiants with metallicities in the range $-3.0 \simeq$ [Fe/H] $\simeq 0.0$, derived by Nissen & Schuster (1991). The calibration is based on the position of a star in the $c_0-(b-y)_0$ and $M_V-(b-y)_0$ diagrams and takes into account the evolutionary status of the star. The second method follows an empirical calibration equation developed by Schuster et al. (2004, 2006) and is based on a sample of 512 stars from the Hipparcos Catalogue (ESA 1997) with parallax errors ≤10%. The calibration equation is a polynomial function of $(b-y)_0$, c_0 and m_0. In Figure 1, a $(b-y)$ vs M_V diagram shows the validity zone for this M_V calibration. This region is not a rectangle but an irregular polygon, and stars inside this calibration zone will have reliable absolute-magnitude values. This calibration equation works very well for main sequence, evolved main sequence, subgiant, metal-poor, and very metal-poor stars, over the range $0.26 \leq (b-y) \leq 0.61$, which corresponds roughly to the spectral types F3V–K4V (Crawford 1975; Olsen 1984). A few stars fall outside the limits of this M_V calibration equation; therefore their M_V and distance values were not reliable from this method. For some of these stars, parallax values were found in the literature, and for those with no parallax value, the M_V and distance values were obtained from the first method mentioned above. Preliminary distance values are listed in Tables 3–4, and the final distance values used in the kinematic analyses, in Tables 5–6.

3.2. *Photometric parameters*

Photometric parameters like $E(b-y)$, [Fe/H] and M_V were obtained using specific calibration equations. In the case of the intrinsic-color calibration, equation (1) reported in Schuster & Nissen (1989) has been used, and iterated to consistency, that is, iterated until changes in the photometric values m_0 and c_0, which are part of this intrinsic-color calibration equation, are less than $0^{\rm m}.0001$, as in previous papers. This empirical equation is valid for F and G stars of intermediate and extreme Populations I and II, covering the ranges: $0.254 \leq (b-y) \leq 0.550$, $0.033 \leq m_1 \leq 0.470$, $0.116 \leq c_1 \leq 0.540$, $2.550 \leq \beta \leq 2.681$, and $-2.49 \leq$ [Fe/H] $\leq +0.22$ (Schuster & Nissen 1989). Once we have obtained the intrinsic color, $(b-y)_0$ for each star, the corresponding $E(b-y)$ has been calculated. If the $E(b-y)$ value was ≥0.015, the m_1 and c_1 indices and V magnitude were also dereddened to m_0, c_0, and V_0 respectively. Metallicity determinations were made following the equations derived by Schuster & Nissen (1989) for F and G stars; for the F-type star [Fe/H] calibration, the ranges of the calibration stars were $0.22 \leq (b-y) \leq 0.38$, $0.03 \leq m_1 \leq 0.21$, $0.17 \leq c_1 \leq 0.58$, and $-3.5 \leq$ [Fe/H] $\leq +0.2$; and for the G-type star [Fe/H] calibration $0.37 \leq (b-y) \leq 0.59$, $0.03 \leq m_1 \leq 0.57$, $0.10 \leq c_1 \leq 0.47$, and $-2.6 \leq$ [Fe/H] $\leq +0.4$ (Schuster & Nissen 1989). Finally, for the M_V determination, the two methods described above (see § 3.1) have been followed, and the range of the second method as in Figure 1.

© Copyright 2012: Instituto de Astronomía, Universidad Nacional Autónoma de México

TABLE 3

PHOTOMETRIC PARAMETERS FOR OUR 72 METAL-POOR STARS

ID	V_0 [mag]	$(b-y)_0$ [mag]	m_0 [mag]	c_0 [mag]	N_u	β [mag]	N_β	$E(b-y)$ [mag]	[Fe/H] [dex]	M_{V_2} [mag]	D_2 [pc]
−13 : 3442	10.154	0.277	0.059	0.381	6	2.621	6	+0.032	−2.42	3.86	181.1
−22 : 1833	11.186	0.526	0.329	0.169	7	2.521	8	···	−1.16	6.97	69.7
−23 : 12296	10.715	0.337	0.065	0.258	7	2.597	7	+0.035	−1.61	4.64	164.2
430-051	12.778	0.370	0.074	0.179	5	2.574	6	−0.004	−1.35	5.33	308.9
440-071	13.212	0.390	0.075	0.123	5	2.566	5	+0.024	−1.73	5.55	340.4
469-098	12.332	0.393	0.072	0.158	5	2.555	5	+0.054	−1.70	5.58	224.5
487-027	12.585	0.333	0.052	0.253	5	2.595	5	+0.000	−2.00	4.66	384.3
492-053	12.681	0.343	0.044	0.219	6	2.586	5	−0.001	−2.22	4.96	349.4
528-161	12.417	0.375	0.059	0.122	2	2.581	2	+0.064	−1.62	5.46	245.8
558-002	12.633	0.312	0.058	0.296	5	2.610	5	+0.015	−1.98	4.37	449.9
636-003	12.812	0.377	0.062	0.200	3	2.581	3	+0.014	−1.55	5.16	339.8
666-038	12.913	0.409	0.120	0.165	5	2.557	5	+0.026	−1.39	5.68	279.1
732-048	12.533	0.316	0.058	0.288	6	2.630	5	+0.011	−1.93	4.42	419.3
736-002	12.253	0.294	0.062	0.351	5	2.615	5	+0.028	−2.00	3.91	465.6
760-071	13.311	0.352	0.063	0.230	2	2.585	2	+0.024	−1.59	4.87	487.0
787-042	12.191	0.420	0.087	0.145	5	2.540	5	···	−1.72	5.87	184.0
802-051	11.276	0.381	0.061	0.173	5	2.561	6	+0.026	−1.77	5.41	148.7
833-020	12.916	0.454	0.122	0.054	5	2.560	5	···	−2.20	5.82	263.1
G14-32	8.374	0.596	0.320	0.371	6	2.540	6	···	−0.38	−1.66	···
G15-10	12.036	0.479	0.058	0.130	4	2.530	4	···	−2.12	5.76	179.6
G17-25	9.612	0.474	0.204	0.163	11	2.536	7	···	−1.35	6.44	43.1
G17-37	13.495	0.562	0.134	0.169	5	2.547	4	···	−2.14	2.93	···
G18-21	13.146	0.445	0.039	0.102	4	2.543	4	···	−2.11	6.27	236.7
G18-40	12.352	0.374	0.061	0.169	6	2.569	6	+0.025	−1.59	5.41	244.7
G19-25	11.703	0.497	0.179	0.130	7	2.530	7	···	−1.83	6.63	103.3
G25-24	11.627	0.378	0.054	0.182	5	2.575	6	+0.012	−1.74	5.31	183.3
G26-12	12.162	0.349	0.037	0.255	5	2.568	5	−0.008	−2.51	4.34	367.5
G26-42	12.531	0.381	0.061	0.223	5	2.573	4	+0.015	−1.81	4.83	346.3
G28-31	12.400	0.349	0.054	0.210	5	2.588	5	+0.050	−1.84	5.06	293.2
G28-34	12.976	0.621	0.406	0.181	5	2.509	5	···	−0.89	5.18	···
G28-48	11.089	0.499	0.367	0.232	6	2.541	7	···	−0.47	6.40	86.6
G29-23	10.229	0.341	0.058	0.326	5	2.586	5	+0.005	−1.76	3.48	223.8
G30-52	8.301	0.449	0.263	0.253	2	2.569	2	+0.047	−0.35	5.81	31.5
G43-05	12.442	0.437	0.079	0.105	6	2.523	6	···	−1.94	6.18	178.5
G44-38	13.466	0.639	0.335	0.120	4	2.489	4	···	−2.09	4.26	···
G58-15	13.072	0.437	0.068	0.125	9	2.548	9	···	−1.94	6.08	249.8
G65-33	12.907	0.627	0.446	0.158	4	2.496	4	···	−0.65	6.29	···
G72-34	12.964	0.564	0.228	0.168	3	2.515	3	···	−1.82	5.09	···
G92-49	11.117	0.414	0.182	0.266	5	2.571	5	+0.267	−0.54	5.20	152.4
G94-66	13.876	0.577	0.161	0.117	3	2.535	3	···	−2.47	4.57	···
G114-42	12.779	0.392	0.114	0.205	7	2.570	7	+0.000	−1.22	5.34	307.5
G116-69	12.787	0.474	0.138	0.130	4	2.540	4	···	−1.81	6.42	187.4
G117-64	12.936	0.365	0.057	0.173	6	2.578	6	+0.018	−1.69	5.35	329.1
G122-43	11.865	0.369	0.063	0.156	5	2.584	5	+0.031	−1.54	5.41	195.1
G126-02	11.132	0.670	0.470	0.142	5	2.492	5	···	−0.34	4.60	···
G126-52	10.888	0.299	0.051	0.339	4	2.608	4	+0.024	−2.43	3.92	247.6
G126-62	9.479	0.331	0.064	0.327	6	2.589	8	−0.003	−1.65	3.69	143.9
G130-41	13.197	0.557	0.210	0.133	2	2.526	2	···	−2.11	5.94	283.2
G137-86	13.132	0.333	0.085	0.264	4	2.582	4	−0.024	−1.21	4.68	490.8
G139-16	12.114	0.396	0.078	0.146	4	2.555	4	+0.101	−1.68	5.64	197.2
G144-28	12.651	0.392	0.076	0.121	2	2.563	2	+0.065	−1.74	5.57	260.6
G149-96	13.665	0.490	0.265	0.070	5	2.522	5	···	−2.14	5.66	399.5
G157-38	12.573	0.356	0.054	0.163	1	2.607	2	+0.001	−1.81	5.36	277.3
G159-48	12.061	0.332	0.053	0.235	2	2.603	2	+0.025	−1.95	4.89	271.6
G165-39	10.067	0.312	0.054	0.364	4	2.602	7	+0.007	−2.12	3.31	224.6
G167-50	13.542	0.482	0.115	0.124	5	2.528	5	···	−1.96	6.36	272.8
G171-15	11.551	0.455	0.074	0.094	5	2.535	5	···	−2.06	6.41	106.7
G171-50	13.073	0.378	0.041	0.179	3	2.568	3	+0.011	−2.19	5.29	359.5
G176-27	11.267	0.508	0.344	0.217	5	2.533	5	···	−0.66	6.60	85.9
G178-41	12.644	0.372	0.056	0.179	5	2.573	5	+0.004	−1.70	5.33	289.9
G188-20	12.265	0.319	0.065	0.258	2	2.628	2	+0.089	−1.70	4.78	314.7
G190-15	11.024	0.485	0.055	0.084	6	2.543	6	···	−2.21	6.54	78.8
G195-35	13.099	0.486	0.067	0.109	5	2.536	5	···	−2.15	6.20	239.8
G199-66	12.672	0.375	0.065	0.175	5	2.590	5	+0.011	−1.50	5.38	287.6
G214-01	12.063	0.434	0.062	0.128	3	2.545	3	···	−1.96	6.03	161.1
G214-05	11.474	0.378	0.056	0.146	5	2.564	5	+0.016	−1.69	5.54	153.9
G267-06	10.825	0.334	0.071	0.242	2	2.606	2	−0.003	−1.48	4.86	156.3
HD101063	9.443	0.496	0.151	0.279	6	2.548	3	···	−1.30	3.10	185.8
HD205650	9.058	0.373	0.096	0.233	5	2.574	4	−0.004	−1.07	4.97	65.7
Wolf 436	12.356	0.375	0.057	0.211	4	2.568	4	+0.005	−1.67	5.00	296.5
Wolf 1143	10.989	0.477	0.120	0.118	2	2.542	2	···	−1.95	6.45	80.8
GCRV 6728	12.487	0.407	0.106	0.120	2	2.566	2	+0.022	−1.63	5.59	239.4

© Copyright 2012: Instituto de Astronomía, Universidad Nacional Autónoma de México

TABLE 4

PHOTOMETRIC PARAMETERS FOR OUR 71 METAL-POOR SUBGIANT STARS

ID	V_0 [mag]	$(b-y)_0$ [mag]	m_0 [mag]	c_0 [mag]	N_u	β [mag]	N_β	$E(b-y)$ [mag]	[Fe/H] [dex]	M_{V_2} [mag]	D_2 [pc]
−01 : 1792	9.234	0.524	0.208	0.283	6	2.544	6	···	−0.99	3.19	···
−18 : 6261	10.825	0.396	0.140	0.289	10	2.577	10	+0.006	−0.81	4.59	176.3
+37 : 1458	8.715	0.392	0.072	0.227	11	2.554	13	+0.047	−1.70	4.83	59.9
405-060	10.699	0.375	0.099	0.266	13	2.575	15	+0.138	−1.03	4.59	166.9
412-048	11.274	0.414	0.215	0.375	11	2.599	12	+0.181	+0.05	4.31	246.8
500-093	12.189	0.475	0.091	0.226	11	2.541	12	···	−1.82	3.91	453.2
615-196	11.331	0.422	0.162	0.243	9	2.555	10	+0.029	−0.85	5.34	157.9
625-044	11.404	0.387	0.104	0.173	5	2.580	5	+0.113	−1.37	5.44	156.2
628-018	10.952	0.409	0.193	0.290	7	2.582	8	+0.156	−0.33	5.00	155.1
685-044	11.178	0.329	0.075	0.283	5	2.606	5	+0.147	−1.41	4.45	221.7
685-047	11.408	0.315	0.057	0.319	4	2.601	4	+0.259	−1.98	3.97	307.0
685-053	11.648	0.391	0.131	0.256	8	2.573	9	+0.137	−0.93	4.94	219.4
685-055	10.940	0.395	0.161	0.250	3	2.587	3	+0.137	−0.66	5.15	144.2
752-017	11.331	0.311	0.046	0.334	5	2.597	5	+0.116	−2.51	3.70	335.7
752-018	11.098	0.406	0.160	0.209	8	2.579	8	+0.078	−0.89	5.48	132.7
753-029	11.135	0.394	0.064	0.244	6	2.552	8	+0.124	−1.83	4.42	220.0
813-013	11.739	0.327	0.055	0.263	9	2.601	9	+0.159	−1.95	4.61	267.0
814-012	11.899	0.296	0.036	0.311	6	2.609	7	+0.157	−3.76	4.30	331.5
814-014	11.003	0.344	0.091	0.301	8	2.595	9	+0.148	−1.10	4.20	229.8
830-004	11.525	0.388	0.112	0.301	10	2.575	11	+0.008	−1.14	4.13	301.1
867-011	11.105	0.406	0.174	0.256	7	2.578	7	+0.184	−0.59	5.21	151.0
G01-30	11.854	0.327	0.058	0.266	12	2.602	13	+0.076	−1.85	4.59	283.8
G101-34	10.743	0.511	0.114	0.263	5	2.548	6	···	−1.76	1.79	···
G102-27	8.875	0.402	0.159	0.341	12	2.577	14	+0.040	−0.54	4.07	91.5
G102-47	10.068	0.409	0.105	0.220	9	2.550	10	+0.056	−1.38	5.19	94.6
G107-43	10.189	0.405	0.154	0.312	9	2.570	11	+0.020	−0.66	4.38	144.9
G107-50	11.394	0.313	0.059	0.322	5	2.603	6	+0.058	−1.91	3.97	305.0
G113-22	9.695	0.405	0.110	0.262	5	2.564	6	+0.011	−1.26	4.62	103.5
G122-57	8.372	0.539	0.273	0.296	12	2.543	13	···	−0.62	3.69	···
G128-58	11.674	0.343	0.087	0.293	9	2.596	10	+0.094	−1.16	4.29	299.9
G141-19	10.034	0.388	0.045	0.201	5	2.550	6	+0.125	−2.00	4.99	101.9
G143-23	11.917	0.340	0.082	0.276	4	2.599	4	+0.060	−1.25	4.49	306.1
G146-76	10.485	0.477	0.080	0.292	9	2.539	9	···	−2.01	1.41	···
G152-67	11.564	0.340	0.057	0.257	7	2.589	7	+0.170	−1.80	4.57	250.3
G153-64	11.014	0.393	0.130	0.222	6	2.574	7	+0.093	−1.03	5.26	141.6
G154-21	9.230	0.381	0.076	0.256	3	2.563	4	+0.105	−1.64	4.46	89.9
G154-25	12.040	0.340	0.072	0.266	6	2.596	6	+0.211	−1.43	4.56	313.3
G16-13	9.951	0.399	0.115	0.281	8	2.570	8	+0.011	−1.16	4.41	128.1
G16-20	10.559	0.378	0.082	0.274	6	2.567	7	+0.059	−1.23	4.26	181.6
G16-28	11.765	0.411	0.151	0.246	6	2.562	6	+0.069	−0.87	5.21	204.5
G16-08	11.233	0.403	0.148	0.230	7	2.571	7	+0.091	−0.89	5.32	152.4
G161-73	10.740	0.358	0.081	0.317	4	2.579	5	+0.022	−1.26	3.73	252.7
G170-47	8.946	0.473	0.041	0.264	3	2.528	4	···	−2.46	1.27	···
G172-16	10.701	0.361	0.094	0.281	14	2.584	16	+0.061	−1.07	4.40	181.7
G179-22	10.674	0.477	0.145	0.258	9	2.538	10	···	−1.28	4.19	197.9
G19-27	8.152	0.424	0.163	0.292	3	2.559	4	+0.002	−0.71	4.68	49.4
G193-33	8.800	0.384	0.144	0.317	8	2.592	9	+0.008	−0.66	4.30	79.6
G196-48	10.262	0.369	0.071	0.275	13	2.570	15	+0.019	−1.40	4.19	164.0
G205-42	9.970	0.440	0.075	0.239	6	2.544	6	···	−1.85	4.07	151.6
G23-14	10.277	0.413	0.128	0.222	4	2.553	5	+0.109	−1.16	5.33	97.5
G23-20	11.214	0.382	0.090	0.241	5	2.567	6	+0.082	−1.42	4.83	189.0
G24-25	10.481	0.395	0.115	0.176	5	2.573	5	+0.021	−1.31	5.50	99.0
G29-20	8.941	0.438	0.189	0.254	5	2.550	6	+0.059	−0.69	5.42	50.5
G33-09	10.394	0.378	0.102	0.268	14	2.573	16	+0.044	−1.01	4.57	146.1
G59-18	10.168	0.476	0.152	0.264	9	2.547	10	···	−1.20	4.22	154.9
G60-26	9.677	0.413	0.130	0.236	11	2.554	12	+0.028	−1.10	5.18	79.3
G80-28	9.767	0.345	0.049	0.275	10	2.580	11	+0.048	−2.04	4.17	131.6
G83-45	12.733	0.400	0.086	0.102	6	2.566	6	+0.164	−1.77	5.49	280.5
G87-27	9.826	0.504	0.288	0.269	5	2.548	6	···	−0.48	5.69	67.1
G09-47	7.686	0.521	0.181	0.398	8	2.549	9	···	−1.01	−0.83	···
G90-03	10.252	0.348	0.048	0.304	5	2.576	6	+0.034	−2.03	3.61	212.9
G95-11	11.322	0.319	0.065	0.338	11	2.599	13	+0.141	−1.69	3.71	332.8
HD132475	8.483	0.372	0.080	0.288	7	2.570	7	+0.019	−1.26	4.05	77.1
HD140283	7.208	0.378	0.035	0.288	9	2.557	10	+0.001	−2.53	3.21	62.9
HD148211	7.701	0.364	0.132	0.316	7	2.583	9	−0.013	−0.67	4.25	49.0
HD189558	7.737	0.389	0.102	0.293	10	2.572	11	+0.009	−1.30	4.12	52.9
HD195137	9.623	0.375	0.132	0.299	2	2.586	3	+0.059	−0.73	4.43	109.4
HD210295	9.575	0.580	0.184	0.366	9	2.540	10	···	−1.37	−5.63	···
HD24341	7.790	0.422	0.184	0.282	14	2.565	16	+0.020	−0.51	5.05	35.3
LTT6194	12.259	0.284	0.065	0.388	4	2.618	4	+0.129	−2.05	3.67	522.6
Ross 740	11.819	0.332	0.029	0.218	3	2.591	3	+0.217	−3.30	5.00	230.7

© Copyright 2012: Instituto de Astronomía, Universidad Nacional Autónoma de México

© Copyright 2012: Instituto de Astronomía, Universidad Nacional Autónoma de México

TABLE 5

KINEMATIC INPUT DATA FOR OUR 136 STARS

ID	R.A. [degrees]	Dec. [degrees]	$V_{\rm rad}$ [km s^{-1}]	μ_α [mas yr^{-1}]	μ_δ [mas yr^{-1}]	$\sigma\ V_{\rm rad}$ [km s^{-1}]	$\sigma\mu_\alpha$ [mas yr^{-1}]	$\sigma\mu_\delta$ [mas yr^{-1}]	D [pc]	σD [pc]	Equinox
−13 : 3442	11.7807359	−14.112068	117.00	0.02500	−0.19670	7.00	0.00160	0.00160	181.1	18.1	2000.0
−22 : 1833	4.8208614	−22.635275	61.00	0.02262	−0.23369	7.00	0.00272	0.00300	69.7	6.9	2000.0
430-051	10.6339558	14.143675	−9.00	−0.01600	−0.18800	7.00	0.00200	0.00600	308.9	30.8	2000.0
440-071	14.5462250	16.016233	80.00	−0.19280	−0.11280	7.00	0.00550	0.00550	340.4	34.0	2000.0
469-098	2.0814647	11.017616	−60.00	0.18260	−0.13900	7.00	0.00380	0.00380	224.5	22.4	2000.0
487-027	9.3189863	13.127525	63.00	0.00670	−0.22070	7.00	0.00240	0.00250	384.3	38.4	2000.0
492-053	11.3985158	9.628252	173.00	0.04540	−0.18700	7.00	0.00380	0.00380	349.9	34.9	2000.0
528-161	1.7333683	6.055958	80.00	0.19890	−0.07900	7.00	0.00480	0.00480	245.8	24.5	2000.0
636-003	20.7503444	−1.682083	−57.00	−0.03830	−0.18610	7.00	0.00550	0.00550	339.8	33.9	2000.0
666-038	9.0802694	−8.282638	295.00	0.09700	−0.14510	7.00	0.00550	0.00550	279.1	27.9	2000.0
732-048	11.2176333	−12.800583	6.00	−0.20580	−0.09030	7.00	0.00550	0.00550	419.3	41.9	2000.0
736-002	12.7376083	−15.766694	−31.00	−0.20790	−0.07400	7.00	0.00450	0.00450	465.6	46.5	2000.0
760-071	22.5611388	−10.796388	−199.00	0.15580	−0.04010	7.00	0.00550	0.00550	487.0	48.7	2000.0
787-042	9.4323100	−16.079913	308.00	−0.22670	−0.04420	7.00	0.00220	0.00240	184.0	18.4	2000.0
802-051	15.2479242	−18.630718	−55.00	−0.27688	−0.37754	7.00	0.00297	0.00202	148.7	14.8	2000.0
833-020	3.9651527	−25.559555	−29.00	0.11420	−0.18900	7.00	0.00550	0.00550	129.9	26.0	2000.0
G14-32	13.1404969	−7.308457	73.80	−0.21979	0.08320	0.60	0.00110	0.00088	212.3	46.4	2000.0
G15-10	15.1627835	−4.751842	89.75	0.06613	−0.46747	0.23	0.00382	0.00290	179.6	17.9	2000.0
G17-25	16.5784316	−4.229070	−171.29	−0.13309	−0.70400	1.93	0.00239	0.00205	48.3	3.5	2000.0
G18-21	22.0762105	11.373647	−286.12	−0.05000	−0.20200	0.27	0.00300	0.00400	236.7	23.6	2000.0
G18-40	22.3315572	5.429797	−192.16	0.31560	0.03800	0.17	0.00450	0.00450	244.7	24.4	2000.0
G19-25	17.4330555	−2.741055	−32.73	−0.09190	−0.34600	0.27	0.00450	0.00450	103.3	10.3	2000.0
G25-24	21.2783333	−1.303333	43.89	0.26630	−0.25110	0.16	0.00150	0.00150	183.3	18.3	2000.0
G26-12	21.5601588	0.395524	−238.91	0.24386	−0.03229	0.17	0.00640	0.00288	367.5	36.7	2000.0
G26-42	22.0064777	1.685072	−107.39	−0.07400	−0.26000	0.29	0.00100	0.00200	346.3	34.6	2000.0
G28-31	23.0662750	−2.542388	−169.32	−0.05190	−0.19000	0.19	0.00440	0.00440	293.2	29.3	2000.0
G28-34	23.0965750	−2.178083	−68.50	0.62000	−0.26000	6.70	0.03000	0.03000	112.3	22.5	2000.0
G28-48	23.2168108	1.803191	25.06	−0.06850	−0.14880	0.25	0.00150	0.00150	86.6	8.6	2000.0
G29-23	23.3279028	3.371301	−246.40	0.30416	−0.14213	0.70	0.00250	0.00191	223.8	22.3	2000.0
G30-52	0.2084199	14.563522	−15.30	0.32176	−0.07131	0.30	0.00167	0.00134	40.1	2.0	2000.0
G43-05	9.8309958	6.609900	99.17	0.06810	−0.32950	0.27	0.00410	0.00400	178.5	17.8	2000.0
G44-38	10.8238575	4.667283	64.95	0.08200	−0.30200	0.19	0.00200	0.00200	79.3	15.9	2000.0
G58-15	10.7778197	22.720519	8.81	0.13670	−0.28310	0.20	0.00550	0.00550	249.8	24.9	2000.0
G65-33	14.2001383	7.103333	−212.10	−0.77000	−0.01000	6.70	0.01500	0.00100	114.0	22.8	2000.0
G72-34	1.7676875	35.913494	−100.73	0.10870	−0.38280	0.19	0.00550	0.00550	135.6	20.3	2000.0
G92-49	20.0560444	−2.955777	−100.35	0.15030	−0.22630	0.21	0.00550	0.00550	152.4	15.2	2000.0
G94-66	2.4316033	17.964200	−118.20	0.10560	−0.21160	0.28	0.00550	0.00550	126.8	15.8	2000.0
G114-42	9.1791416	−3.802722	−86.78	0.13020	−0.25800	0.33	0.00550	0.00550	307.5	30.7	2000.0
G116-69	9.9617697	32.613133	200.88	−0.37390	−0.27760	0.28	0.00550	0.00550	187.4	18.7	2000.0
G117-64	10.0229961	28.767277	−58.29	−0.10650	−0.25700	0.16	0.00550	0.00550	329.1	32.9	2000.0
G122-43	11.7382150	40.538325	−2.90	−0.11075	−0.25290	0.13	0.00218	0.00157	195.1	19.5	2000.0
G126-02	21.4852886	12.183002	−247.00	0.15532	−0.46083	5.00	0.00979	0.00669	38.9	11.9	2000.0
G126-52	22.0703830	19.548458	−241.86	−0.00340	−0.29820	0.19	0.00110	0.00110	247.6	24.7	2000.0
G126-62	22.1920482	18.092826	−291.31	0.50720	0.05760	0.55	0.00130	0.00130	143.9	14.4	2000.0
G130-41	0.0934683	29.181194	−115.49	0.07410	−0.24000	0.28	0.00550	0.00550	283.2	28.3	2000.0

© Copyright 2012: Instituto de Astronomía, Universidad Nacional Autónoma de México

TABLE 5 (CONTINUED)

ID	R.A. [degrees]	Dec. [degrees]	$V_{\rm rad}$ [km s^{-1}]	μ_α [mas yr^{-1}]	μ_δ [mas yr^{-1}]	σ $V_{\rm rad}$ [km s^{-1}]	$\sigma\mu_\alpha$ [mas yr^{-1}]	$\sigma\mu_\delta$ [mas yr^{-1}]	D [pc]	σD [pc]	Equinox
G137-86	16.1709025	9.139444	−83.93	−0.22020	−0.08700	0.14	0.00500	0.00500	490.8	49.0	2000.0
G139-16	17.1631633	8.073788	40.77	−0.10000	−0.41000	0.24	0.01400	0.00700	197.2	19.7	2000.0
G144-28	20.7070000	11.290000	−14.60	−0.10474	−0.36528	0.27	0.01000	0.01000	260.6	26.0	2000.0
G149-96	13.5214508	21.801813	53.86	−0.28200	0.01600	0.35	0.00400	0.00200	399.5	39.9	2000.0
G157-38	23.2681250	−10.919388	−28.00	−0.06980	−0.24930	7.00	0.00550	0.00550	277.3	27.7	2000.0
G159-48	2.2278415	−0.088527	163.03	0.26030	−0.10620	0.32	0.00550	0.00550	271.6	27.1	2000.0
G165-39	13.9859675	33.860933	−171.10	0.08909	−0.42920	0.40	0.00139	0.00120	224.6	22.4	2000.0
G167-50	15.5920988	27.850625	−27.57	−0.37000	−0.17600	0.25	0.00200	0.00400	272.8	27.2	2000.0
G171-15	23.7507522	44.667666	−333.25	0.05130	−0.22820	0.20	0.00190	0.00180	106.7	10.6	2000.0
G171-50	0.3344105	42.729566	−192.19	0.17330	−0.17380	0.24	0.00550	0.00550	359.5	35.9	2000.0
G176-27	11.3646111	50.625758	−28.90	0.25340	−0.23970	0.30	0.00280	0.00250	85.9	8.5	2000.0
G178-41	14.6677916	45.299661	−0.28	−0.28350	0.04200	0.16	0.00330	0.00330	289.9	28.9	2000.0
G188-20	21.7029216	30.996697	−115.65	−0.11830	−0.26500	0.23	0.00400	0.00400	314.7	31.4	2000.0
G190-15	23.2274503	39.417388	−54.67	0.17538	−0.31355	1.08	0.00186	0.00138	78.8	7.8	2000.0
G195-35	9.6384736	48.445391	−126.22	0.21600	−0.25000	0.25	0.00400	0.00300	239.8	23.9	2000.0
G199-66	13.3420147	56.580047	−144.94	−0.28890	−0.12430	0.17	0.00550	0.00550	287.6	28.7	2000.0
G214-01	21.7987866	33.107552	−119.53	0.19790	−0.01350	0.14	0.00210	0.00180	161.1	16.1	2000.0
G214-05	21.9862172	41.041397	−235.27	−0.29190	−0.19260	0.12	0.00180	0.00170	153.9	15.3	2000.0
G267-06	23.9810033	−28.854214	61.00	−0.06810	−0.27433	7.00	0.00278	0.00102	156.3	15.6	2000.0
Wolf 436	12.7837950	1.636627	47.00	−0.18090	−0.02900	7.00	0.00540	0.00540	296.5	29.6	2000.0
Wolf 1143	21.9211519	32.644778	−177.90	0.76205	0.13038	2.00	0.00137	0.00236	80.8	8.0	2000.0
GCRV 6728	10.8414205	56.441902	−130.47	0.17000	−0.39600	0.34	0.00300	0.00400	239.4	23.9	2000.0
HD101063	11.6278896	−28.851346	182.80	−0.31368	−0.01482	0.20	0.00122	0.00072	185.8	18.5	2000.0
HD205650	21.6238979	−27.635188	−102.10	0.34228	−0.20803	0.21	0.00119	0.00069	65.7	6.5	2000.0
−01:1792	7.6639199	−1.522325	51.90	0.18620	−0.24391	1.90	0.00178	0.00062	60.6	8.0	2000.0
+37:1458	6.2670896	37.721880	242.18	0.07224	−0.35130	0.12	0.00142	0.00081	59.9	5.9	2000.0
405-060	0.5415655	18.498000	−181.00	−0.00870	−0.17390	7.00	0.00140	0.00140	166.9	16.6	2000.0
412-048	3.4897361	18.915194	−9.00	0.10120	−0.12130	7.00	0.00550	0.00550	246.8	24.6	2000.0
500-093	14.4838861	13.674250	−26.00	−0.07100	−0.05010	7.00	0.00550	0.00550	453.2	45.3	2000.0
625-044	16.7205666	−1.925138	42.00	−0.06150	−0.20660	7.00	0.00160	0.00180	156.2	15.6	2000.0
628-018	17.5572222	−3.113333	−62.00	−0.02880	−0.02270	7.00	0.00220	0.00240	155.1	15.5	2000.0
685-044	16.6993777	−7.876250	−7.00	−0.23220	−0.17060	7.00	0.00310	0.00330	221.7	22.1	2000.0
685-047	16.6861833	−5.948472	−55.00	−0.09430	−0.16410	7.00	0.00310	0.00330	307.0	30.7	2000.0
685-053	16.4070722	−3.983222	−22.00	−0.01600	−0.16600	7.00	0.00380	0.00380	219.4	21.9	2000.0
752-017	19.4238722	−11.949416	−225.00	−0.04530	−0.16510	7.00	0.00310	0.00310	270.1	40.5	2000.0
752-018	19.4295444	−11.165861	32.00	−0.03530	−0.11500	7.00	0.00180	0.00190	132.7	13.2	2000.0
753-029	19.8342638	−13.322861	−60.00	−0.10950	−0.18440	7.00	0.00220	0.00230	220.0	22.0	2000.0
813-013	19.7285166	−15.927000	26.00	−0.04740	−0.23300	7.00	0.00550	0.00550	267.0	26.7	2000.0
814-012	20.0312472	−15.907944	174.00	−0.12030	−0.15720	7.00	0.00550	0.00550	280.4	28.0	2000.0
814-014	20.0466250	−15.076111	−11.00	−0.01620	−0.19080	7.00	0.00230	0.00250	229.8	22.9	2000.0
867-011	18.5601611	−24.252444	7.00	−0.02670	−0.11970	7.00	0.00320	0.00310	151.0	15.1	2000.0
G01-30	0.8672555	6.957750	−148.02	0.01990	−0.21300	0.20	0.00550	0.00550	283.8	28.3	2000.0
G101-34	6.3344015	38.345587	219.93	0.10114	−0.18296	0.30	0.00296	0.00165	165.8	41.4	2000.0
G102-27	5.7612171	14.688919	38.30	0.06315	−0.18993	0.16	0.00149	0.00095	91.5	9.1	2000.0
G102-47	6.0993159	7.317539	96.87	0.08920	−0.24388	0.26	0.00199	0.00131	94.6	9.4	2000.0
G107-43	7.0353227	36.949663	80.44	−0.06490	−0.21110	0.27	0.00250	0.00250	144.9	14.4	2000.0
G107-50	7.1646902	42.653708	148.37	0.01500	−0.25600	0.19	0.00190	0.00190	305.0	30.5	2000.0

© Copyright 2012: Instituto de Astronomía, Universidad Nacional Autónoma de México

TABLE 5 (CONTINUED)

ID	R.A. [degrees]	Dec. [degrees]	$V_{\rm rad}$ [km s^{-1}]	μ_α [mas yr^{-1}]	μ_δ [mas yr^{-1}]	$\sigma\ V_{\rm rad}$ [km s^{-1}]	$\sigma\mu_\alpha$ [mas yr^{-1}]	$\sigma\mu_\delta$ [mas yr^{-1}]	D [pc]	σD [pc]	Equinox
G113-22	8.2827161	0.017700	53.81	0.22440	−0.15040	0.22	0.00090	0.00090	103.5	10.3	2000.0
G122-57	11.9666891	48.203455	47.25	−0.24435	−0.12581	0.15	0.00102	0.00079	40.3	8.1	2000.0
G128-58	23.4249305	30.107027	−142.90	0.25870	0.03810	0.20	0.00550	0.00550	299.9	29.9	2000.0
G141-19	18.5546789	13.157080	101.20	−0.04077	−0.27435	3.00	0.00204	0.00179	101.9	10.1	2000.0
G143-23	20.0345277	15.130138	−55.56	−0.14950	−0.21600	0.18	0.00550	0.00550	306.1	30.6	2000.0
G146-76	10.9992994	44.778819	−115.12	−0.10180	−0.21980	0.20	0.00130	0.00130	260.1	65.0	2000.0
G152-67	15.9619444	−2.523333	−47.00	−0.23700	−0.15900	7.00	0.03000	0.03000	250.3	25.0	2000.0
G153-64	16.5416750	−8.560555	114.78	−0.15010	−0.20750	0.28	0.00250	0.00280	141.6	14.1	2000.0
G154-21	17.7961322	−9.605125	−129.00	−0.14469	−0.20948	10.00	0.00193	0.00107	89.9	8.9	2000.0
G154-25	17.8436111	−16.986666	200.00	−0.06050	−0.21640	7.00	0.00550	0.00550	313.3	31.3	2000.0
G16-13	15.8497041	8.423265	−51.54	−0.23503	−0.15964	0.10	0.00220	0.00233	128.1	12.8	2000.0
G16-20	15.9718391	2.051697	170.09	−0.08530	−0.24030	0.19	0.00170	0.00160	181.6	18.1	2000.0
G16-28	16.0602894	2.618338	3.05	−0.14410	−0.16840	0.25	0.00180	0.00180	204.5	20.4	2000.0
G16-08	15.7611111	−2.260000	−35.00	−0.29170	−0.09510	6.70	0.00170	0.00170	152.4	15.2	2000.0
G161-73	9.7605083	−4.674583	120.92	0.15110	−0.25660	0.16	0.00220	0.00240	252.7	25.2	2000.0
G170-47	17.5448958	23.736564	−284.20	−0.33226	−0.08780	0.10	0.00060	0.00094	106.7	26.7	2000.0
G172-16	0.6429666	47.630569	−84.98	0.29410	0.02020	0.24	0.00230	0.00220	181.7	18.1	2000.0
G179-22	15.2406070	33.010630	96.08	0.01126	−0.20333	0.24	0.00140	0.00152	197.9	19.7	2000.0
G19-27	17.5237230	−2.538810	3.94	−0.27340	−0.10693	0.06	0.00106	0.00054	75.1	7.2	2000.0
G193-33	7.1749413	53.251778	−28.83	−0.07267	−0.24132	0.20	0.00135	0.00092	79.6	7.9	2000.0
G196-48	10.8490616	53.247552	133.87	−0.22217	−0.18934	0.79	0.00116	0.00103	164.0	16.4	2000.0
G205-42	18.9047096	42.983438	−269.16	0.03892	0.25422	0.14	0.00086	0.00119	151.6	15.1	2000.0
G23-14	19.8637799	5.612733	18.46	−0.14042	−0.23174	0.23	0.00771	0.00597	97.5	9.7	2000.0
G23-20	20.0093648	9.353532	−267.12	−0.19399	−0.19669	0.26	0.00349	0.00241	189.0	18.9	2000.0
G24-25	20.6711388	0.555497	−307.15	0.14160	−0.14430	0.48	0.00140	0.00140	99.0	9.9	2000.0
G29-20	23.3003325	9.074475	−190.36	0.41250	−0.12430	0.19	0.00160	0.00160	50.5	5.0	2000.0
G33-09	0.7592885	16.971612	−91.87	0.02022	−0.21710	0.25	0.00143	0.00192	146.1	14.6	2000.0
G59-18	12.3919502	16.902566	31.70	−0.28100	−0.12970	0.40	0.00140	0.00130	154.9	15.4	2000.0
G60-26	12.6664926	12.642247	112.94	−0.00199	−0.31704	0.25	0.00209	0.00145	79.3	7.9	2000.0
G80-28	3.8651506	−3.819639	133.40	0.27240	0.00685	3.20	0.00177	0.00160	131.6	13.1	2000.0
G83-45	4.9259083	16.211972	170.02	0.19880	−0.26690	0.38	0.00550	0.00550	280.5	28.0	2000.0
G87-27	7.1689744	37.276080	−48.67	0.00547	−0.25610	0.21	0.00195	0.00122	67.1	6.7	2000.0
G09-47	9.1119238	20.509864	170.15	−0.07922	−0.18566	0.18	0.00140	0.00095	102.0	30.6	2000.0
G90-03	7.4974567	32.866194	29.09	0.01693	−0.19964	0.28	0.00244	0.00148	212.9	21.2	2000.0
G95-11	3.1679091	34.847552	205.26	0.24950	−0.00460	0.34	0.00520	0.00620	332.8	33.2	2000.0
HD132475	14.9971566	−22.012722	176.40	−0.56047	−0.49947	0.20	0.00112	0.00092	77.1	7.7	2000.0
HD140283	15.7175268	−10.933497	−169.00	−1.11560	−0.30278	0.20	0.00093	0.00083	57.3	3.2	2000.0
HD148211	16.4535830	−22.126796	−15.50	−0.27685	−0.30100	0.20	0.00112	0.00104	52.7	2.7	2000.0
HD189558	20.0167348	−12.255650	−13.00	−0.30916	−0.36529	0.20	0.00110	0.00103	67.8	5.0	2000.0
HD195137	20.5016150	−16.236977	14.00	−0.27540	−0.10740	6.70	0.00160	0.00160	109.4	10.9	2000.0
HD210295	22.1615128	−13.605408	−19.00	−0.03979	−0.08460	10.00	0.00158	0.00078	192.9	57.9	2000.0
HD24341	3.9142197	52.419864	143.00	0.10759	−0.14905	0.40	0.00152	0.00115	65.1	4.5	2000.0
LTT6194	15.5093333	−29.655916	218.48	−0.06460	−0.17480	0.70	0.00550	0.00550	522.6	52.2	2000.0
Ross 740	19.5934388	−4.170861	−197.00	−0.16640	−0.25690	7.00	0.00550	0.00550	185.8	18.5	2000.0

© Copyright 2012: Instituto de Astronomía, Universidad Nacional Autónoma de México

TABLE 6

KINEMATIC OUTPUT DATA FOR OUR 136 STARS

ID	U' [km s^{-1}]	V' [km s^{-1}]	W' [km s^{-1}]	$\sigma U'$ [km s^{-1}]	$\sigma V'$ [km s^{-1}]	$\sigma W'$ [km s^{-1}]	D [pc]	σD [pc]	[Fe/H] [dex]	$V_{\rm rot}$ [km s^{-1}]	X
−13 : 3442	122.19	−157.37	−12.90	9.91	10.42	11.64	181.1	18.1	−2.42	62.63	+31.37
−22 : 1833	31.71	−67.71	−41.83	7.16	6.25	4.42	69.7	6.9	−1.16	152.29	−4.37
430-051	105.74	−228.11	−83.00	10.50	25.95	10.49	308.9	30.8	−1.35	−8.11	+20.19
440-071	−44.88	−317.56	158.69	12.35	35.12	10.82	340.4	34.0	−1.73	−97.56	+39.11
469-098	−38.50	−231.74	16.58	9.84	23.06	6.85	224.5	22.4	−1.70	−11.74	+27.34
487-027	121.43	−368.14	−74.04	16.01	35.65	13.31	384.3	38.4	−2.00	−148.14	+50.86
492-053	191.18	−288.78	90.10	21.81	23.84	9.91	349.9	34.9	−2.22	−68.78	+44.70
528-161	−164.72	−167.84	−60.69	14.83	21.60	6.57	245.8	24.5	−1.62	52.16	+17.47
636-003	151.46	−255.97	−52.06	19.51	24.77	12.01	339.8	33.9	−1.55	−35.97	+27.64
666-038	59.01	−337.08	126.36	20.63	14.49	7.24	279.1	27.9	−1.39	−117.08	+35.17
732-048	−254.84	−234.45	−251.72	28.63	26.11	27.92	419.3	41.9	−1.93	−14.45	+32.08
736-002	−322.95	−310.45	−138.98	33.60	35.48	15.01	465.6	46.5	−2.00	−90.45	+43.33
760-071	−320.93	−241.23	−41.65	28.70	19.98	22.99	487.0	48.7	−1.59	−21.23	+26.48
787-042	−215.59	−273.82	−27.13	12.25	6.66	16.38	184.0	18.4	−1.72	−53.82	+33.21
802-051	−75.86	−291.28	−96.48	7.10	31.82	8.45	148.7	14.8	−1.77	−71.28	+36.44
833-020	86.49	−89.94	57.67	13.24	23.94	8.04	129.9	26.0	−2.20	130.06	+18.37
G14-32	−180.76	−84.93	130.26	47.65	14.85	13.55	212.3	46.4	−0.38	135.07	−17.01
G15-10	274.94	−249.91	−163.65	20.09	25.93	23.36	179.6	17.9	−2.12	−29.91	+37.72
G17-25	−78.74	−157.62	−128.80	4.65	10.29	4.24	48.3	3.5	−1.35	62.38	+10.99
G18-21	101.18	−337.46	70.49	17.20	13.11	10.29	236.7	23.6	−2.11	−117.46	+48.96
G18-40	−363.16	−161.27	−43.40	32.38	5.51	18.10	244.7	24.4	−1.59	58.73	+16.04
G19-25	52.21	−150.31	−44.72	7.20	15.53	4.73	103.3	10.3	−1.83	69.69	+19.19
G25-24	−24.59	−126.10	−278.71	5.93	16.94	26.26	183.3	18.3	−1.74	93.90	+14.32
G26-12	−387.47	−212.83	−168.08	29.66	7.81	32.26	367.5	36.7	−2.51	7.17	+40.33
G26-42	276.52	−350.89	−52.97	30.70	29.43	13.06	346.3	34.6	−1.81	−130.89	+44.99
G28-31	167.53	−260.27	63.40	19.72	18.83	8.93	293.2	29.3	−1.84	−40.27	+33.73
G28-34	−219.98	−234.12	−126.12	46.51	44.45	39.47	112.3	22.5	−0.89	−14.12	+12.19
G28-48	66.89	−5.25	−31.21	5.41	3.52	1.93	86.6	8.6	−0.47	214.75	−25.69
G29-23	−214.18	−355.63	14.81	20.77	22.08	18.78	223.8	22.3	−1.76	−135.63	+44.65
G30-52	−33.76	−31.97	0.73	2.37	1.87	0.95	40.1	2.0	−0.35	188.03	−24.49
G43-05	127.33	−262.85	4.72	16.69	22.28	7.41	178.5	17.8	−1.94	−42.85	+35.98
G44-38	72.67	−102.06	29.13	15.85	16.39	6.15	79.3	15.9	−2.09	117.94	+17.86
G58-15	264.37	−254.18	47.60	26.39	27.31	4.47	249.8	24.9	−1.94	−34.18	+34.85
G65-33	−376.54	−239.86	−54.51	58.25	54.52	25.94	114.0	22.8	−0.65	−19.86	+8.36
G72-34	54.59	−206.08	−149.74	4.03	23.65	30.26	135.6	20.3	−1.82	13.92	+26.28
G92-49	−45.64	−150.95	−126.49	3.27	11.05	16.80	152.4	15.2	−0.54	69.05	−5.34
G94-66	84.93	−153.83	18.20	2.53	16.06	8.44	126.8	15.8	−2.47	66.17	+31.86
G114-42	379.46	−187.70	−78.85	33.15	26.99	8.37	307.5	30.7	−1.22	32.30	+12.43
G116-69	−320.86	−300.05	−45.67	21.45	28.90	21.37	187.4	18.7	−1.81	−80.05	+38.35
G117-64	8.48	−384.38	−172.25	7.86	41.98	14.34	329.1	32.9	−1.69	−164.38	+47.07
G122-43	6.54	−239.74	27.08	1.89	25.47	2.30	195.1	19.5	−1.54	−19.74	+25.33
G126-02	−55.05	−235.72	52.64	8.97	16.30	20.89	38.9	11.9	−0.34	−15.72	+1.91
G126-52	170.41	−363.14	−103.76	20.65	16.97	22.55	247.6	24.7	−2.43	−143.14	+58.41
G126-62	−342.90	−269.64	−17.23	30.03	3.96	17.28	143.9	14.4	−1.65	−49.64	+31.33
G130-41	82.36	−255.59	−212.95	7.97	18.53	28.95	283.2	28.3	−2.11	−35.59	+38.27

© Copyright 2012: Instituto de Astronomía, Universidad Nacional Autónoma de México

TABLE 6 (CONTINUED)

ID	U' [km s^{-1}]	V' [km s^{-1}]	W' [km s^{-1}]	$\sigma U'$ [km s^{-1}]	$\sigma V'$ [km s^{-1}]	$\sigma W'$ [km s^{-1}]	D [pc]	σD [pc]	[Fe/H] [dex]	$V_{\rm rot}$ [km s^{-1}]	X
G137-86	−108.66	−482.54	229.05	10.05	48.58	28.89	490.8	49.0	−1.21	−262.54	+50.72
G139-16	259.56	−287.67	−51.63	22.14	33.17	13.31	197.2	19.7	−1.68	−67.67	+34.25
G144-28	350.91	−280.10	−124.18	36.33	29.26	17.96	260.6	26.0	−1.74	−60.10	+34.41
G149-96	−416.77	−281.46	145.82	44.06	30.18	8.60	399.5	39.9	−2.14	−61.46	+42.22
G157-38	232.71	−241.14	−30.72	23.93	25.44	9.46	277.3	27.7	−1.81	−21.14	+30.66
G159-48	−243.68	−275.84	−85.73	17.81	32.47	5.78	271.6	27.1	−1.95	−55.84	+37.86
G165-39	363.27	−303.29	−137.60	37.48	27.61	1.99	224.6	22.4	−2.12	−83.29	+44.69
G167-50	−51.04	−455.95	244.57	6.45	45.97	25.89	272.8	27.2	−1.96	−235.95	+61.56
G171-15	140.04	−313.51	−10.25	1.93	2.98	11.28	106.7	10.6	−2.06	−93.51	+44.88
G171-50	−85.01	−361.60	−239.60	19.57	22.07	32.41	359.5	35.9	−2.19	−141.60	+53.63
G176-27	135.45	−43.29	51.23	11.22	5.22	6.84	85.9	8.5	−0.66	176.71	−17.10
G178-41	−281.28	−207.67	151.72	29.39	22.53	14.54	289.9	28.9	−1.70	12.33	+24.20
G188-20	382.29	−198.52	−121.58	39.16	10.50	17.14	314.7	31.4	−1.70	21.48	+23.00
G190-15	17.73	−82.28	−99.59	0.79	4.76	12.45	78.8	7.8	−2.21	137.72	+17.56
G195-35	270.00	−262.99	118.13	17.83	26.39	20.47	239.8	23.9	−2.15	−42.99	+40.00
G199-66	−180.16	−395.86	8.71	23.20	35.09	13.18	287.6	28.7	−1.50	−175.86	+44.94
G214-01	−110.04	−118.09	−64.05	10.96	1.89	10.49	161.1	16.1	−1.96	101.91	+17.47
G214-05	269.28	−206.21	73.71	25.29	1.01	2.44	153.9	15.3	−1.69	13.79	+23.82
G267-06	156.75	−139.96	−38.01	13.68	15.95	7.01	156.3	15.6	−1.48	80.04	+11.16
Wolf 436	−174.34	−169.83	28.19	20.85	18.31	7.44	296.5	29.6	−1.67	50.17	+18.69
Wolf 1143	−261.93	−177.23	−84.45	25.52	2.95	14.31	80.8	8.0	−1.95	42.77	+24.99
GCRV 6728	283.76	−381.26	163.79	20.78	36.04	26.18	239.4	23.9	−1.63	−161.26	+45.52
HD101063	−188.08	−250.90	14.31	23.51	11.38	8.81	185.8	18.5	−1.30	−30.90	+22.21
HD205650	−120.16	−80.11	3.09	9.16	7.40	10.87	65.7	6.5	−1.07	139.89	−4.47
−01 : 1792	28.51	−83.01	30.98	7.75	8.68	1.96	60.6	8.0	−0.99	136.99	−5.62
+37:1458	−240.23	−63.67	22.69	1.23	9.62	2.62	59.9	5.9	−1.70	156.33	+5.41
405-060	129.59	−176.55	36.02	6.58	8.78	10.90	166.9	16.6	−1.03	43.45	+7.35
412-048	−8.82	−167.98	−13.62	7.33	19.17	7.07	246.8	24.6	+0.05	52.02	−14.37
500-093	−37.27	−167.51	13.40	11.61	21.60	8.68	453.2	45.3	−1.82	52.49	+21.25
625-044	105.02	−118.82	−10.94	8.44	14.47	5.07	156.2	15.6	−1.37	101.18	+6.31
628-018	−39.42	−30.72	0.71	6.37	3.78	2.67	155.1	15.5	−0.33	189.28	−25.04
685-044	10.42	−275.01	95.55	6.51	29.00	9.96	221.7	22.1	−1.41	−55.01	+27.45
685-047	22.06	−262.77	−33.17	8.96	27.23	5.41	307.0	30.7	−1.98	−42.77	+36.73
685-053	59.71	−130.18	−76.38	9.30	14.71	8.78	219.4	21.9	−0.93	89.82	−0.61
752-017	−100.43	−278.93	20.37	14.51	30.02	7.00	270.1	40.5	−2.51	−58.93	+48.95
752-018	69.37	−39.04	−10.29	6.88	7.50	2.19	132.7	13.2	−0.89	180.96	−13.26
753-029	68.56	−205.14	50.09	12.45	19.75	3.90	220.0	22.0	−1.83	14.86	+26.35
813-013	133.97	−251.75	−61.63	12.32	28.53	9.26	267.0	26.7	−1.95	−31.75	+34.72
814-012	288.51	−133.13	0.30	15.16	22.99	9.38	280.4	28.0	−3.76	86.87	+53.77
814-014	67.68	−177.47	−49.96	8.92	19.10	7.11	229.8	22.9	−1.10	42.53	+8.81
867-011	28.03	−68.50	−14.30	6.96	8.80	3.21	151.0	15.1	−0.59	151.50	−15.14
G01-30	161.94	−268.38	−30.28	12.74	22.30	16.54	283.8	28.3	−1.85	−48.38	+34.98
G101-34	−217.46	−130.77	56.76	3.09	40.90	2.89	165.8	41.4	−1.76	89.23	+15.31
G102-27	−6.82	−75.61	−15.45	2.03	8.21	1.91	91.5	9.1	−0.54	144.39	−15.17
G102-47	−36.26	−126.58	−20.57	4.33	10.62	1.88	94.6	9.4	−1.38	93.42	+7.51
G107-43	−95.31	−104.61	−56.48	2.92	12.00	8.98	144.9	14.4	−0.66	115.39	−9.10
G107-50	−194.02	−326.82	−25.63	6.71	35.53	9.06	305.0	30.5	−1.91	−106.82	+43.75

© Copyright 2012: Instituto de Astronomía, Universidad Nacional Autónoma de México

TABLE 6 (CONTINUED)

ID	U' [km s^{-1}]	V' [km s^{-1}]	W' [km s^{-1}]	$\sigma U'$ [km s^{-1}]	$\sigma V'$ [km s^{-1}]	$\sigma W'$ [km s^{-1}]	D [pc]	σD [pc]	[Fe/H] [dex]	$V_{\rm rot}$ [km s^{-1}]	X
G113-22	67.62	−92.42	82.74	9.44	7.23	5.75	103.5	10.3	−1.26	127.58	+0.76
G122-57	−37.73	−15.96	49.61	6.47	8.33	0.32	40.3	8.1	−0.62	204.04	−21.43
G128-58	−310.18	−221.90	1.34	35.29	12.12	10.20	299.9	29.9	−1.16	−1.90	+15.75
G141-19	175.09	−6.83	−14.13	9.38	9.10	4.04	101.9	10.1	−2.00	213.17	+3.71
G143-23	290.33	−247.45	39.46	31.88	22.25	8.25	306.1	30.6	−1.25	−27.45	+20.80
G146-76	15.75	−291.96	−83.35	12.00	73.66	2.68	260.1	65.0	−2.01	−71.96	+41.11
G152-67	−54.52	−314.92	70.61	22.22	48.06	30.39	250.3	25.0	−1.80	−94.92	+40.10
G153-64	134.36	−142.47	57.81	2.33	17.07	1.58	141.6	14.1	−1.03	77.53	+2.90
G154-21	−81.64	−126.07	−4.56	9.90	10.69	2.01	89.9	8.9	−1.64	93.93	+12.40
G154-25	273.93	−263.08	−59.23	9.81	32.55	11.77	313.3	31.3	−1.43	−43.08	+26.28
G16-13	−28.08	−160.07	26.94	1.04	16.40	5.57	128.1	12.8	−1.16	59.93	+7.68
G16-20	216.64	−159.19	71.99	7.71	20.11	4.35	181.6	18.1	−1.23	60.81	+8.90
G16-28	44.53	−195.83	32.08	3.40	21.14	2.64	204.5	20.4	−0.87	24.17	+6.81
G16-08	−78.17	−177.65	81.93	8.04	19.01	10.52	152.4	15.2	−0.89	42.35	+4.83
G161-73	258.45	−266.55	38.77	29.66	19.53	4.43	252.7	25.2	−1.26	−46.55	+23.49
G170-47	−134.94	−285.08	5.16	6.77	28.74	31.94	106.7	26.7	−2.46	−65.08	+48.80
G172-16	−167.03	−184.27	34.05	21.87	12.86	1.88	181.7	18.1	−1.07	35.73	+9.12
G179-22	195.35	−57.21	86.36	15.48	11.19	0.79	197.9	19.7	−1.28	162.79	−3.45
G19-27	25.20	−65.92	72.33	1.12	7.88	6.10	75.1	7.2	−0.71	154.08	−13.19
G193-33	−6.58	−65.82	−47.91	4.16	7.29	4.37	79.6	7.9	−0.66	154.18	−14.16
G196-48	−187.10	−138.44	91.72	12.90	18.52	2.77	164.0	16.4	−1.40	81.56	+9.44
G205-42	−241.88	−188.14	−36.40	17.55	4.20	3.78	151.6	15.1	−1.85	31.86	+24.51
G23-14	111.96	−60.19	8.97	9.14	8.98	3.37	97.5	9.7	−1.16	159.81	−5.35
G23-20	28.66	−331.56	118.40	19.05	14.80	6.72	189.0	18.9	−1.42	−111.56	+35.02
G24-25	−189.96	−233.65	47.54	0.92	4.44	8.40	99.0	9.9	−1.31	−13.65	+20.15
G29-20	−66.30	−167.72	95.50	7.05	5.32	5.16	50.5	5.0	−0.69	52.28	−0.29
G33-09	90.69	−137.51	−31.33	4.88	9.79	10.53	146.1	14.6	−1.01	82.49	+1.88
G59-18	−120.11	−173.94	−0.74	12.97	18.14	3.94	154.9	15.4	−1.20	46.06	+10.26
G60-26	81.73	−109.73	87.02	6.12	9.78	2.99	79.3	7.9	−1.10	110.27	−0.03
G80-28	−161.20	−115.22	28.96	7.68	10.83	11.07	131.6	13.1	−2.04	104.78	+18.62
G83-45	−122.33	−438.51	−33.35	3.72	44.67	7.05	280.5	28.0	−1.77	−218.51	+55.66
G87-27	47.54	−62.24	−33.02	0.88	7.73	2.51	67.1	6.7	−0.48	157.76	−18.06
G09-47	−110.65	−129.65	62.71	0.94	24.94	15.33	102.0	30.6	−1.01	90.35	+0.85
G90-03	−14.34	−184.91	−27.45	1.01	19.67	5.08	212.9	21.2	−2.03	35.09	+27.52
G95-11	−377.68	−162.69	131.31	22.04	27.75	21.21	332.8	33.2	−1.69	57.31	+18.14
HD132475	67.63	−300.31	68.93	8.16	25.97	3.20	77.1	7.7	−1.26	−80.31	+27.89
HD140283	−238.27	−237.43	50.72	6.03	14.60	7.63	57.3	3.2	−2.53	−17.43	+43.92
HD148211	−14.59	−85.48	5.97	0.55	5.21	0.31	52.7	2.7	−0.67	134.52	−11.40
HD189558	85.29	−112.75	51.01	6.34	8.97	2.87	67.8	5.0	−1.30	107.25	+4.18
HD195137	118.59	−46.67	97.81	11.03	7.32	10.21	109.4	10.9	−0.73	173.33	−15.32
HD210295	60.29	−55.55	21.26	18.33	19.12	7.71	192.9	57.9	−1.37	164.45	−1.95
HD24341	−140.57	41.59	−8.90	1.99	3.29	1.06	65.1	4.5	−0.51	261.59	−31.04
LTT6194	148.81	−454.36	−138.78	8.46	41.86	25.97	522.6	52.2	−2.05	−234.36	+63.07
Ross 740	6.20	−312.03	75.62	16.74	22.45	5.68	185.8	18.5	−3.30	−92.03	+68.34

© Copyright 2012: Instituto de Astronomía, Universidad Nacional Autónoma de México

The errors of these photometric metallicities are discussed in detail by Schuster & Nissen (1989), which is the calibration paper for the [Fe/H] values derived here. These errors are smallest near the solar metallicity where the m_0 photometric parameter is most effected by line blanketing, and largest for the low metallicities of the halo stars due to decreasing line blanketing and decreasing changes in such for a given change in metallicity. According to Schuster & Nissen (1989), the estimated standard deviation of a single photometric determination of [Fe/H] by our method is ±0.06 dex at approximately [Fe/H] = −0.5 dex, ±0.10 at [Fe/H] ≈ −1.5, and ±0.25 at [Fe/H] ≈ −2.5.

Final photometric parameters for the LM stars are presented in Table 3, and the corresponding parameters for the SG stars are shown in Table 4. A brief description of columns in both tables is the following:

Column 1: identification name of the star, as in Tables 1 and 2.

Columns 2, 3, 4, 5: the V_0 magnitude, and the indices $(b-y)_0$, m_0, and c_0, respectively, on the standard system, corrected for interstellar reddening when $E(b-y) \geq 0.015$. Otherwise, the observed standard values are given without correction.

Column 6: total number of independent observations for the indices $(b-y)_0$, m_0, and c_0; the same as Column 7 in Tables 1 and 2.

Column 7: the β value on the standard system.

Column 8: total number of independent observations for β.

Column 9: the calculated color excess for the star, $E(b-y)$, due to interstellar reddening.

Column 10: the metallicity, [Fe/H], calculated from the photometric calibration equations.

Columns 11, 12: estimated absolute magnitude and distance from the second method described above; when the star falls outside the calibration region shown in Figure 1, no distance is given in Column 12.

In the process of obtaining the photometric parameters, some stars were slightly outside the limits of the calibration equations. Depending on the object, one (or more) of the following extrapolations were applied: in the intrinsic-color calibration equation, in the metallicity calibrations, and/or in the absolute-magnitude calibration equation. These extrapolations were small, $\lesssim 0\overset{m}{.}03$, and were checked for consistency. In particular, extending the limits for the metallicity calibration equation was important because it is used in the absolute-magnitude calculation (first method) and therefore useful for the photometric-distance estimation; also, the metallicity occurs in the [Fe/H] vs $V_{\rm rot}$ diagram.

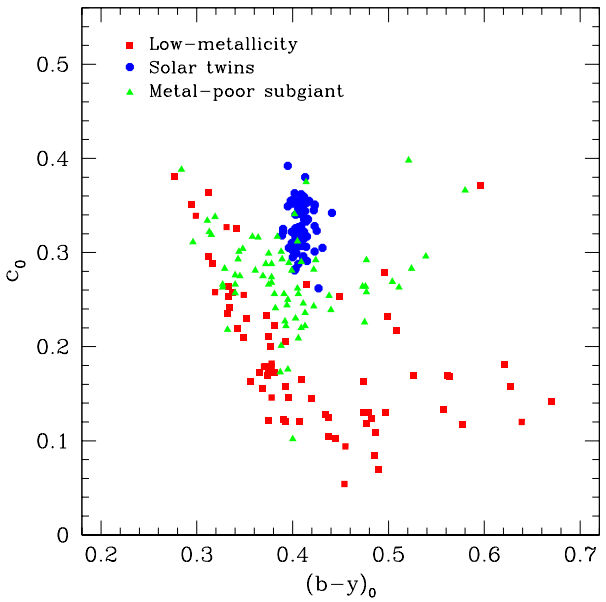

Fig. 2. The $(b-y)_0$ versus c_0 diagram for the metal-poor and subgiant stars of this paper, plus the solar twins from Meléndez et al. (2010). Symbols as in Figure 1. These data have been dereddened as discussed in the text.

In Figure 2 is shown the $(b-y)_0$ versus c_0 diagram for the three samples of stars: the metal-poor stars and metal-poor subgiants of this paper, and the solar twins from Meléndez et al. (2010). The solar twins are seen to be a very compact and homogeneous group, with a small range in $(b-y)_0$, as discussed in that paper (Meléndez et al. 2010). The metal-poor stars (subgiants and others) show rather clearly a main-sequence–turn–off-subgiant arrangement, but displaced downward in this diagram with respect to the solar twins, as would be expected for metal-poor stars (Nissen & Schuster 1991). In fact, this displacement of about $-0\overset{m}{.}15$ corresponds to a metallicity difference of about −2.0 dex according to equation (2) of Nissen & Schuster (1991), which agrees approximately with the more metal-poor stars of Table 3 at $(b-y)_0 \approx 0.41$. Also, a few of the metal-poor subgiant candidates, such as G24-25, G25-44, G83-45, and Ross 740 appear along the metal-poor main sequence, and so do not remain as good subgiant candidates according to this photometric classification. However, it should be noted that G24-25 has been discovered to be a typical CH giant with an unseen companion, large over-abundances of C and the heavy *s*-process elements, and mild over-abundances of Eu and the

© Copyright 2012: Instituto de Astronomía, Universidad Nacional Autónoma de México

light *s*-process elements (Liu et al. 2011). These over-abundances and the companion readily explain this photometric mis-classification as main sequence when G24-25 is really a giant. The effects of anomalous C abundances, via the CH and CN bands, upon the c_0 photometric index have been detected and discussed in several papers (Začs, Nissen, & Schuster 1998; Grundahl et al. 2000; Schuster et al. 2004).

3.3. *Kinematic parameters*

In order to plot the three different diagrams that involve the Galactic space velocities (U', V', W'), the radial-velocity and proper-motion values for each star in both samples (LM and SG) had to first be obtained from the literature. The proper motions and coordinates used in this paper have been taken primarily from three sources: Hipparcos (ESA 1997), Tycho-2 (Høg et al. 2000), and the revised NLTT (Salim & Gould 2003). For a few stars other sources have been employed, such as the original NLTT (Luyten 1979a), the LHS (Luyten 1979b), the Lowell Proper Motion Survey (Giclas, Slaughter, & Burnham 1959; Giclas, Burnham, & Thomas 1961, 1975), and the PPM Star Catalogue (Röser & Bastian 1991). In general the proper-motion errors range from 0.5–3.0 mas yr^{-1} per component for the best sources, such as Hipparcos and Tycho-2, to as large as $\gtrsim$10 mas yr^{-1} per component for the other sources, such as the NLTT and the Lowell Proper Motion Survey.

The radial velocities for the present study have been obtained from the literature, from a number of sources, such as Carney et al. (1994), Barbier-Brossat, Petit, & Figon (1994), Barbier-Brossat & Figon (2000), Nordström et al. (2004), Ryan & Norris (1991), Fouts & Sandage (1986), and Abt & Biggs (1972). The observational errors of these velocities range from a few tenths of a km s^{-1} for the best sources, such as Carney et al. (1994) and Nordström et al. (2004), to $\approx$7 km s^{-1} for the older sources. For binary stars the radial velocity of the center of mass (the γ velocity) has been used whenever an orbital solution exists, such as from these sources: Latham et al. (1988, 1992, 2002) and Goldberg et al. (2002).

Once we have found radial-velocity and proper-motion values, we have joined them to the position and distance data and used a computer program kindly loaned by C. Allen to calculate the Galactic space velocities. The input parameters for this program are given in Table 5: the equatorial coordinates, the radial velocity, the proper motions in right ascension and declination, the errors of these, the final distance and its error, and the equinox of the coordinates. This program is based on the precepts, matrix equations, and Galactic coordinate system given by Johnson & Soderblom (1987); our version of this program has been modified to also accept stellar positions with equinoxes of 1991.25 and 2000.0. In this system, U', V', and W' are positive toward the Galactic center, in the galactic-rotation direction, and to the north galactic pole, respectively. Galactic velocity values (U, V, W) were corrected for the solar motion using the following values $(U', V', W') = (U, V, W) + (+10.0, +14.9, +7.7)$ km s^{-1}, and our typical (median) errors in these velocities are $(\pm6.2, \pm6.6, \pm4.8)$ km s^{-1} for the 1533 stars of the previous three catalogues; $(\pm10.7, \pm18.5, \pm8.4)$ km s^{-1} for the 136 stars of this paper. These errors have been estimated using the matrix equations of Johnson & Soderblom (1987), which consider all covariances of the errors to be null. However, the results of Montes et al. (2001) show that ignoring such covarinaces generally decreases the estimated errors by only 0.1 km s^{-1} for the large majority of cases, and by about 1.2 km s^{-1} in the worst of cases, for stars with the largest errors in the input kinematic data. Since it was not possible to find radial velocity and proper-motion values for 7 stars (4 LM stars and 3 SG stars), Galactic space velocities are reported for only 136 stars from the original 143 stars in the sample. Final values of U', V' and W' are presented in Table 6, along with their estimated errors, the final distances used, photometric [Fe/H] values, $V_{\rm rot} = V' + 220$ km s^{-1}, and the stellar-population parameter, X, from Schuster et al. (1993), where $X > 0.00$ indicates a probable halo star.

Since kinematic and photometric parameters available in the catalogues of Schuster & Nissen (1988), Schuster et al. (1993) and Schuster et al. (2006) were obtained following the same procedures and calibrations, and therefore are consistent with the new data presented in this work, our sample has been enlarged considerably by joining the parameters from these previous catalogues to our new values. In this way, our sample grew from 143 stars to 1676 objects with Galactic velocities. In the process of joining these catalogues, stars in common between all catalogues have been identified, and the final sample has been cleaned of these repeated stars. When repeat photometric observations were made for the same star, the new and old observations were combined taking into account the air masses of the observations. Besides, since some stars have been reported in the literature as binary or variable stars, our final sample has been analyzed in two ways, including the

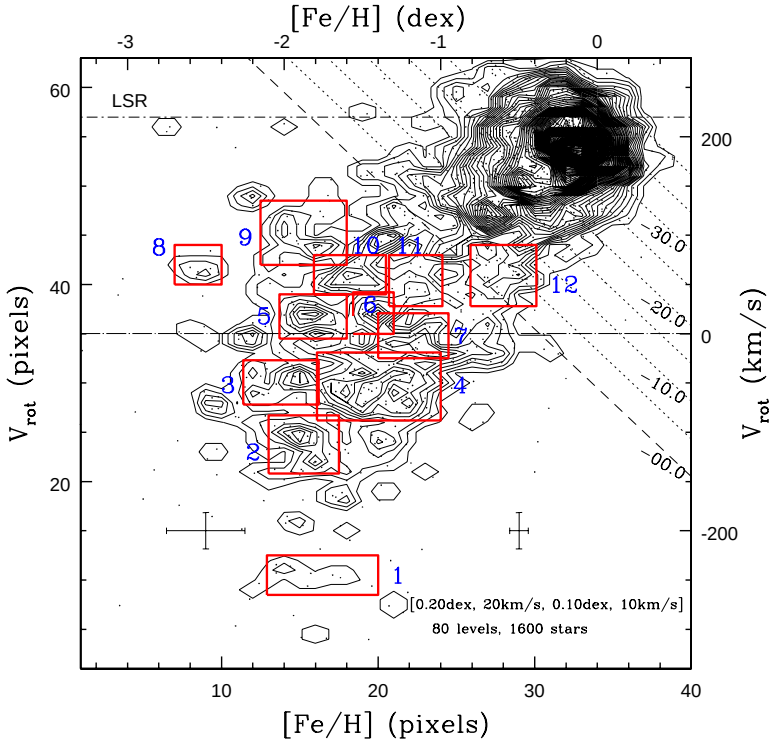

Fig. 3. $V_{\rm rot}$ versus [Fe/H] diagram for the full sample of 1600 high-velocity and metal-poor stars at high resolution with kernel sizes of 20 km s^{-1} and 0.20 dex, and step sizes of 10 and 0.10, respectively. Since the errors for low-metallicity values are larger than those for high-metallicity, we show typical error bars corresponding to the more extreme cases. The velocity error bar is the same in both cases. Eighty contour levels have been used. Diagonal lines show constant X values, our stellar population criterion from Schuster et al. (1993), where $X = 0.00$ provides a good separation between the Galactic halo and the high-velocity disk. Twelve candidate regions are shown by (red) rectangles.

binaries and variable stars (a final sample of 1637 stars) and excluding them (1319 stars).

4. KINEMATIC ANALYSIS

Having enlarged our sample of stars with Galactic velocity values, the [Fe/H] vs $V_{\rm rot}$, Bottlinger (V' vs U'), and Toomre (V' vs $(U'^2 + W'^2)^{1/2}$) diagrams have been plotted. In these diagrams we look for groupings of stars sharing similar kinematical and metallicity properties. To facilitate this, on each diagram number-density contours were overlaid. Contours were obtained using an algorithm written in the AWK programming language, used by Schuster et al. (2006), and loaned to us by A. Moitinho. The original code has been modified slightly to fulfill our specific necessities. Input data for the code were: axes limits, a kernel size, and a step size. Contours were produced by passing a given kernel over the full extent of the particular diagram. The kernel is a simple rectangle which is shifted one half of its width between each count when scanning a given diagram horizontally, and one half of its length for each shift vertically. In order to obtain "high-" or "low-resolution" contours, kernel sizes of 0.20 dex by 20 km s^{-1} have been used for the [Fe/H] vs $V_{\rm rot}$ diagram (with step sizes of 0.10 dex and 10 km s^{-1}), and also 0.30 dex by 40 km s^{-1} kernels (with step sizes of 0.15 dex and 20 km s^{-1}), respectively. For the purely kinematic diagrams, the "high-" or "low-resolution" kernel sizes were 20 by 20 km s^{-1} (10 and 10 km s^{-1}), and 30 by 40 km s^{-1} (15 and 20 km s^{-1}), respectively.

The [Fe/H] vs $V_{\rm rot}$ diagram should show the remnants of clusters or accretion events by the Galaxy which have conserved their metallicity and orbital angular momentum, which should apply to first order for many halo stars except perhaps those traveling to the most inner kiloparsecs of the Galaxy; in these inner regions interactions with the Galactic bar and bulge will necessarily disperse these groups more rapidly in angular momentum ($V_{\rm rot}$). Likewise, the Toomre diagram will show groups conserving their Galactic orbital energy with dispersal again being most rapid for those groups transversing the most

© Copyright 2012: Instituto de Astronomía, Universidad Nacional Autónoma de México

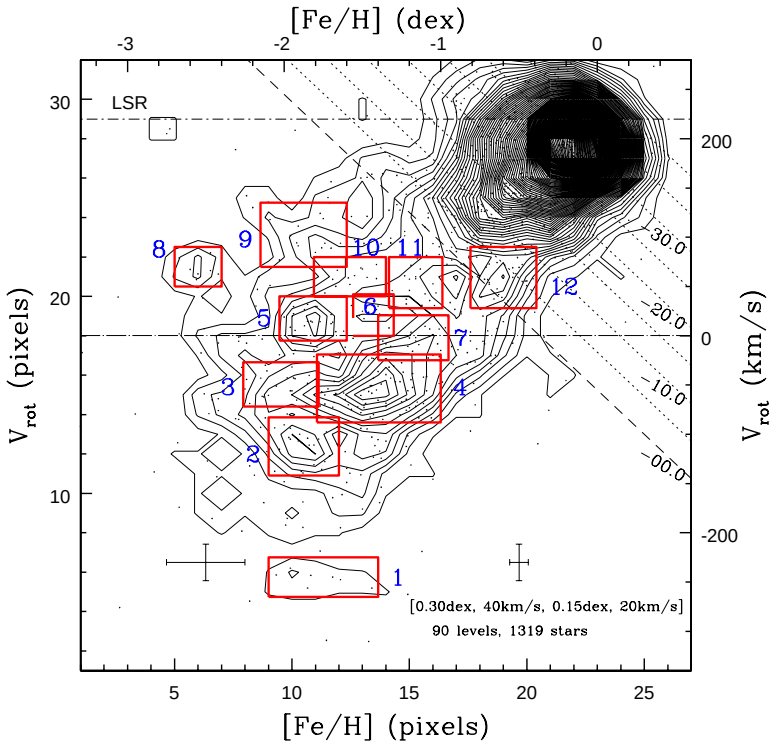

Fig. 4. Low-resolution $V_{\rm rot}$ versus [Fe/H] diagram for our cleaned sample of stars (1319) with kernel sizes of 40 km s^{-1} and 0.30 dex, and step sizes of 20 and 0.15, respectively. As in Figure 3, error bars are shown for low- and high-metallicity values. The velocity error bar is the same in both cases.

central few kiloparsecs of the Galaxy. The Bottlinger diagram is one of the classic tools for detecting moving groups projected onto the Galactic plane (Eggen 1958, 1965, 1971, 1977, 1983b, 1996b,c; Eggen & Sandage 1959).

These three diagrams place little emphasis upon the vertical velocity, W', and none upon its sign, being squared for the Toomre diagram. However, the loss of information is minimal due to more efficient phase mixing of the Galactic orbits in the vertical direction (in the direction of the Galactic poles) than in the horizontal (Galactic-plane) directions. For example, the results of Dehnen (1998), derived from more than 14,000 stars observed by the *Hipparcos* satellite, show considerable structure in the (v_x, v_y) plane, similar to a Bottlinger diagram, but these moving groups are much less visible when v_z, similar to W', is plotted. This is attributed to differences in the efficiency of phase mixing, vertical versus horizontal.

4.1. *[Fe/H],$V_{\rm rot}$ diagram*

Although high- and low-resolution contour plots were obtained for our total sample of stars (including binaries and variables) as well as for our cleaned sample (without binaries and variables), only Figures 3 and 4 are shown as examples. In our complete sample, it was not possible to determine photometric metallicities, [Fe/H], for 37 stars; thus the total numbers of stars plotted in these diagrams are 1600 and 1319, respectively. In the purely kinematical Bottlinger and Toomre plots only our-cleaned sample, low-resolution plots are shown, Figures 5 and 6. In actuality only about 605 of these stars are good halo candidates according to the diagonal, dashed cut of Figure 3, $X \geq 0.00$, Schuster et al. (1993). The rotation velocity of the LSR about the Galactic center is taken to be 220 km s^{-1}, so that $V_{\rm rot} = V' + 220$ km s^{-1}. As in Schuster et al. (2006), in these diagrams two horizontal lines have been plotted locating the LSR velocity $V_{\rm rot} = +220$ and the 0 km s^{-1} velocity. As well, various lines for different values of the "X" parameter, defined by Schuster et al. (1993) and used in Schuster et al. (2006) to separate halo, $X \geq 0.0$, from "high-velocity disk" stars, $X < 0.00$, have been drawn.

Comparing the two sets of plots, moving-group candidates have been taken as those structures present in all four diagrams. Sometimes, while a candidate group looks like an isolated group of contours

© Copyright 2012: Instituto de Astronomía, Universidad Nacional Autónoma de México

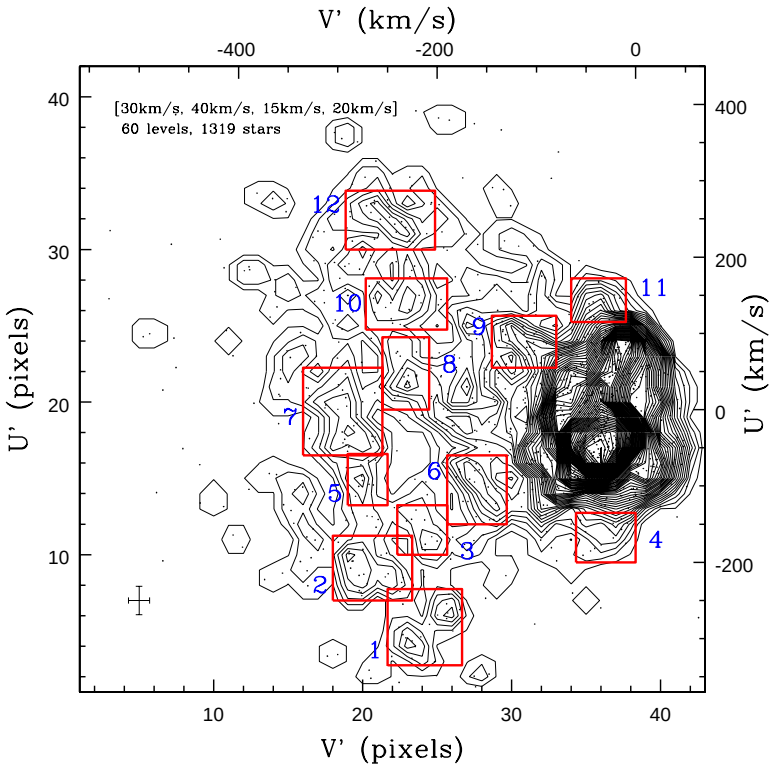

Fig. 5. Bottlinger diagram for the cleaned sample of 1319 high-velocity and metal-poor stars, at low resolution with kernel sizes of 40 and 30 km s^{-1}, and step sizes of 20 and 15, respectively. Typical (median) error bars are shown for both velocity components. Sixty contour levels have been used in this figure. Again, twelve candidate regions for moving groups are shown by (red) rectangles.

("isles") in the high-resolution plot, the same group looks like an attached group of contours ("peninsulas") in the corresponding low-resolution diagram. With this in mind, the presence of the 12 most significant moving-group candidates have been identified in our four [Fe/H], $V_{\rm rot}$ diagrams. Distinguishing "peaks" (i.e. "isles" or "peninsulas") versus "valleys" in these contour diagrams has been easily accomplished by overplotting as small points the actual stellar postions in each diagram. Table 7 shows the limits in [Fe/H] and $V_{\rm rot}$ for the location of each candidate region. In all four [Fe/H],$V_{\rm rot}$ diagrams, each candidate region has been enclosed in a rectangular (red) box and labeled with its corresponding number from Table 7. These rectangular boxes have been drawn to emphasize our candidate groups, and very roughly correspond to $\pm 1.5\sigma$ for the velocity components in these diagrams, and $\pm$ 2.0σ for the metallicity component. So, there is some risk that stellar members of the classic moving groups, such as those of Eggen, will not correspond exactly to our candidate groups due to these statistical limits of our rectangular boxes and due to the poorer quality of the older kinematic and metallicity values. Indeed, as discussed below, four of the original Kapteyn stars of Eggen fall just outside our G03-37 (A3+B4) candidate group.

In Schuster et al. (2006) a similar stellar-density-contour technique was used in this [Fe/H] vs $V_{\rm rot}$ diagram to detect two probable components to the Galactic thick disk. One has ([Fe/H], $V_{\rm rot}$) $\approx$ (-0.4 dex, $+160$ km s^{-1}), and the other ([Fe/H], $V_{\rm rot}$) $\approx$ (-0.7, $+120$). This latter thick-disk moving group has now been tentatively identified as the Arcturus group studied by Eggen (1971, 1983b) and by Navarro et al. (2004), who have assigned [Fe/H] ≈ -0.6 and $V_{\rm rot}$ $\approx +90 - 110$ km s^{-1} to this thick-disk component. In this paper we are studying mainly the structure in the Galactic halo, but some of our analyses overlap the thick disk, such as the candidate-group No. 12 of Figures 3–4 and of Table 7. Three of the Arcturus-group members, as listed by Eggen (1971, 1983b), are found in this candidate-group No. 12, although it is not centered well on the coordinates, ([Fe/H], $V_{\rm rot}$) $\approx$ (-0.7, $+120$), given above. (Three members are also found

© Copyright 2012: Instituto de Astronomía, Universidad Nacional Autónoma de México

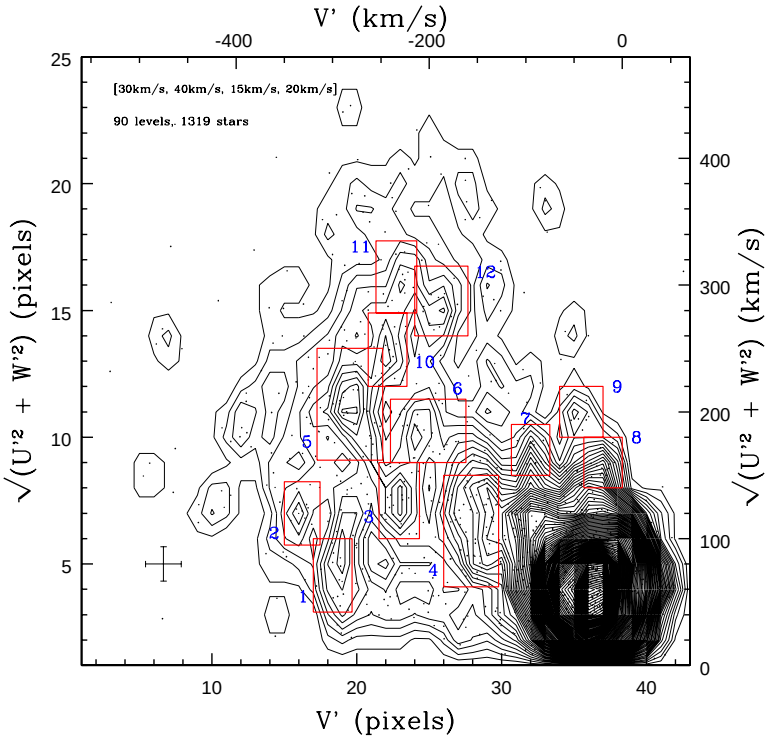

Fig. 6. Toomre diagram for the cleaned sample of 1319 high-velocity and metal-poor stars, at low resolution with kernel sizes of 40 and 30 km s^{-1}, and step sizes of 20 and 15, respectively. Typical (median) error bars are shown for both axes. Ninety contour levels have been used. Again, twelve candidate regions for moving groups are shown by (red) rectangles.

in the candidate-group No. 9 of Figure 5 and Table 8 for the Bottlinger diagram; this halo candidate group has a mean rotational velocity of +108 km s^{-1}, but is offset about 45 km s^{-1} in U' from that of the Arcturus group (Eggen 1971).

4.2. *Bottlinger and Toomre diagrams*

In a similar way, contour plots have been obtained with two different resolutions in both the Bottlinger and Toomre diagrams, and the same process has been followed for identifying possible candidate groups. A representative Bottlinger diagram is shown in Figure 5 for low-resolution contours and the cleaned sample (without binaries). Comparing the four Bottlinger diagrams, the 12 most significant candidate groups have been identified and listed in Table 8. These groups are shown in the diagram as (red) boxes labeled according to Table 8. A representative Toomre diagram is presented in Figure 6, again for the low-resolution contours and the cleaned sample. In the four Toomre diagrams, again 12 candidate moving-groups have been identified, and these are shown in Table 9. As in the [Fe/H], $V_{\rm rot}$ and Bottlinger diagrams, candidate groups are identified with a rectangular (red) box and a sequence number

TABLE 7

CANDIDATE GROUPS FROM THE [Fe/H] vs $V_{\rm rot}$ DIAGRAM

Region	[Fe/H] [dex]		$V_{\rm rot}$ [km s^{-1}]	
	min	max	min	max
1	−2.10	−1.40	−265	−225
2	−2.10	−1.65	−142	−83
3	−2.26	−1.78	−72	−27
4	−1.79	−1.00	−88	−19
5	−2.03	−1.60	−5	+40
6	−1.56	−1.30	0	+42
7	−1.40	−0.95	−25	+20
8	−2.70	−2.40	+50	+90
9	−2.15	−1.60	+70	+135
10	−1.81	−1.35	+40	+80
11	−1.33	−0.99	+28	+80
12	−0.81	−0.39	+28	+90

© Copyright 2012: Instituto de Astronomía, Universidad Nacional Autónoma de México

© Copyright 2012: Instituto de Astronomía, Universidad Nacional Autónoma de México

TABLE 8

CANDIDATE GROUPS FROM THE BOTTLINGER DIAGRAM

Region	V' [km s^{-1}]		U' [km s^{-1}]	
	min	max	min	max
1	−250	−175	−335	−235
2	−305	−225	−250	−165
3	−240	−190	−190	−125
4	−60	0	−200	−135
5	−290	−250	−125	−58
6	−190	−130	−150	−60
7	−335	−255	−60	+55
8	−255	−208	0	+95
9	−145	−80	+55	+123
10	−272	−190	+105	+172
11	−65	−10	+115	+172
12	−292	−202	+210	+287

TABLE 9

CANDIDATE GROUPS FROM THE TOOMRE DIAGRAM

Region	V' [km s^{-1}]		$(U'^2 + W'^2)^{1/2}$ [km s^{-1}]	
	min	max	min	max
1	−320	−280	42	100
2	−350	−313	95	145
3	−252	−210	100	160
4	−185	−128	62	145
5	−316	−248	162	250
6	−240	−162	160	210
7	−115	−75	150	190
8	−40	0	140	180
9	−65	−20	180	220
10	−263	−223	220	278
11	−255	−213	278	335
12	−215	−160	260	315

consistent with Table 9. The identification of the 12 most significant candidate groups has been done independently for each of these three figures: [Fe/H], $V_{\rm rot}$, Bottlinger, and Toomre.

5. MOVING-GROUP CANDIDATES

Once the candidate groups have been recognized within each of the three kinematic-metallicity diagrams, these have been compared, and stars in common among the different groups identified. The [Fe/H], $V_{\rm rot}$ group has been taken as reference. When a star from a group in this reference list was present in at least one of the other two lists of groups, it has been selected as an overlapping star. All groups showed overlapping stars with the exception of Group 1 from the [Fe/H], $V_{\rm rot}$ list.

Because of the small number of member stars in each group, a minimum of four overlapping stars has been required to select a group as a good moving-group candidate. The candidate groups with stars present in the three kinematic diagrams have been labeled with an "A" followed by a sequence number, and groups with stars appearing in only two of the three diagrams with a "B" plus a sequence number. In Tables 10 and 11, our moving-group candidates are listed along with their kinematic data. The first 2 and the last 3 columns of these tables are of particular interest: in Columns 1 and 2 the labels given to each group, as well as the individual star identifications, appear, respectively; the last 3 columns show the region numbers to which the star belongs in each diagram list, Tables 7–9. It is worth noticing that some of our "B" moving-group candidates seem to be an extension of one of the "A" candidates, having in common the same regions of the two diagrams which define the respective "B" candidates: group B3 an extension of Group A1, Group B5 of A2, B4 of A3, and B6 of A7. These groups were combined and the final groups were named according to the first (usually non-binary) Giclas star in the original "A" group. Groups B1 and B2 were not considered the best moving-group candidates because of their larger ranges in both the U' and W' velocity components, but, as discussed in the text, phase-mixing and Galactic accretion processes tend to scatter these two velocities more, and the $V_{\rm rot}$ and [Fe/H] values of the members of B1 and B2 are also very similar to those of the ω Cen group identified by Meza et al. (2005) (see below, § 6). Final moving-group names are as follows: Group G18-39 (A1+B3), Group G21-22 (A2+B5), Group G03-37 (A3+B4), Group G01-35 (A7+B6), Group G18-24 (A4), Group G22-20 (A5), and Group G56-39 (A6). These groups are our best moving-group candidates, and these are shown in Table 12.

In next section the possible coincidences of our moving-group candidates with moving groups reported in the literature are discussed.

TABLE 10

MOVING GROUP CANDIDATES (A GROUPS)

Group	ID	U' [km s^{-1}]	V' [km s^{-1}]	W' [km s^{-1}]	[Fe/H] [dex]	$V_{\rm rot}$ [km s^{-1}]	$(U'^2+W'^2)^{1/2}$ [km s^{-1}]	[Fe/H],$V_{\rm rot}$ [Regions]	Bott [Regions]	Toomre [Regions]
A1	−48 : 2445	−217.17	−278.56	−10.50	−1.67	−58.56	217.42	4	2	5
	490-061	−198.54	−285.49	+24.15	−1.40	−65.49	200.00	4	2	5
	709-053	−188.83	−288.69	+103.87	−1.48	−68.69	215.51	4	2	5
	787-042*	−215.59	−273.82	−27.13	−1.72	−53.82	217.29	4	2	5
	G18-39	−190.57	−256.36	−17.39	−1.40	−36.36	191.36	4	2	5
	G31-26	−217.88	−304.88	+113.66	−1.37	−84.88	245.74	4	2	5
	G36-47	−183.01	−274.73	−79.54	−1.49	−54.73	199.55	4	2	5
	G66-30[b]	−198.74	−271.86	+7.39	−1.57	−51.86	198.88	4	2	5
	G70-33	−207.69	−287.04	+61.44	−1.25	−67.04	216.59	4	2	5
	G86-39	−237.17	−278.35	−24.19	−1.44	−58.35	238.40	4	2	5
	G87-13	−198.27	−284.49	+15.80	−1.22	−64.49	198.90	4	2	5
	G120-15	−239.44	−276.54	+12.81	−1.46	−56.54	239.78	4	2	5
	G157-85	−185.83	−288.49	−66.24	−1.35	−68.49	197.28	4	2	5
	G176-53	−228.07	−270.48	+60.61	−1.44	−50.48	235.99	4	2	5
	G187-30[b]	−227.66	−299.24	−34.54	−1.28	−79.24	230.27	4	2	5
	HD101063*	−188.08	−250.90	+14.31	−1.30	−30.90	188.62	4	2	5
A2	G146-56	223.58	−263.03	+26.68	−1.32	−43.03	225.17	4	12	5
	HIP36878	212.66	−275.82	+90.99	−1.21	−55.82	231.31	4	12	5
	G02-38[b]	219.81	−257.90	−53.68	−1.28	−37.90	226.27	4	12	10
	G21-22	249.46	−257.09	−29.61	−1.24	−37.09	251.21	4	12	10
	G82-42	212.29	−245.10	−136.78	−1.29	−25.10	252.54	4	12	10
A3	G03-37	−54.45	−290.10	+37.76	−1.59	−70.10	66.26	4	7	1
	G05-36	−38.72	−292.97	−55.34	−1.20	−72.97	67.54	4	7	1
	G142-44	−46.48	−291.65	+63.09	−1.35	−71.65	78.36	4	7	1
	G170-56	−48.66	−288.86	−28.28	−1.11	−68.86	56.28	4	7	1
	G272-122	−43.54	−294.72	+32.70	−1.57	−74.72	54.45	4	7	1
	HIP22068	+0.58	−299.93	+81.28	−1.43	−79.93	81.28	4	7	1
	HIP69232	+46.92	−292.18	−1.75	−1.53	−72.18	46.95	4	7	1
A4	G18-24[b]	−242.57	−209.15	−196.75	−1.49	+10.85	312.33	6	1	12
	G179-54[b]	−301.04	−201.00	+87.39	−1.44	+19.00	313.47	6	1	12
	G195-34	−269.12	−199.48	−20.68	−1.52	+20.52	269.91	6	1	12
	G202-65[b]	−302.61	−215.51	−9.22	−1.41	+4.49	302.75	6	1	11
A5	G22-20	93.04	−213.17	+46.14	−1.01	+6.83	103.85	7	8	3
	G90-37	76.09	−239.83	+110.72	−1.05	−19.83	134.35	7	8	3
	G232-18	74.16	−241.16	+100.10	−1.01	−21.16	124.58	7	8	3
	HIP90261	44.87	−229.00	−102.25	−1.14	−9.00	111.66	7	8	3
A6	G56-39	−90.96	−167.30	+4.09	−1.05	+52.70	91.05	11	6	4
	G59-18*	−120.11	−173.94	−0.74	−1.20	+46.06	120.11	11	6	4
	G83-26	−101.29	−148.57	+102.81	−1.19	+71.43	144.32	11	6	4
	G269-87	−96.35	−152.24	−1.37	−1.13	+67.76	96.36	11	6	4
A7	558-008	−64.69	−145.71	−41.49	−0.64	+74.29	76.85	12	6	4
	G01-35	−119.32	−150.54	−14.45	−0.50	+69.46	120.19	12	6	4
	G07-10	−88.21	−180.45	+96.04	−0.74	+39.55	130.40	12	6	4
	G57-07	−70.85	−160.65	−49.72	−0.54	+59.35	86.56	12	6	4
	G99-21	−60.97	−181.06	+23.69	−0.61	+38.94	65.41	12	6	4

[b]Identified as a binary star by SIMBAD.
*Star from our photometric catalogues in Table 1 or 2.

© Copyright 2012: Instituto de Astronomía, Universidad Nacional Autónoma de México

6. DISCUSSION

One of the most prolific authors pioneering in moving-group identification was O. J. Eggen. As we have mentioned, although most of his studies were centered about moving groups in the disk of our Galaxy, in his publications he reported specific member names and kinematics for three moving groups in the halo, *Ross 451*, *Groombridge 1830*, and *Kapteyn*. In his publications, he lists the specific member names and kinematics for each one of these groups. Average galactic velocity components for them are $(U', V', W') \sim (-135, -329.5, +162)$, $(-253, -136, -14)$, and $(+23, -273.5, -8)$ km s^{-1}, respectively.

In order to analyze the effect of the binary systems included in the complete sample, we have searched for kinematical groups both in our complete and cleaned samples of stars. Since no considerable effect on the grouping structure shown by the number density contours was found, we decided to

TABLE 11

MOVING GROUP CANDIDATES (B GROUPS)

Group	ID	U' [km s^{-1}]	V' [km s^{-1}]	W' [km s^{-1}]	[Fe/H] [dex]	$V_{\rm rot}$ [km s^{-1}]	$(U'^2+W'^2)^{1/2}$ [km s^{-1}]	[Fe/H],$V_{\rm rot}$ [Regions]	Bott [Regions]	Toomre [Regions]
B1	G01-30*	+161.94	−268.38	−30.28	−1.85	−48.38	164.74	3	···	5
	G28-31*	+167.53	−260.27	+63.40	−1.84	−40.27	179.12	3	···	5
	492-053*	+191.18	−288.78	+90.10	−2.22	−68.78	211.35	3	···	5
	G10-54	+193.68	−263.54	−52.00	−1.93	−43.54	200.54	3	···	5
	G130-41*	+82.36	−255.59	−212.95	−2.11	−35.59	228.32	3	···	5
	G10-04	−113.46	−282.10	−116.86	−2.13	−62.10	162.88	3	···	5
B2	G59-27[b]	−67.61	−240.61	−134.25	−1.64	−20.61	150.31	4	···	3
	G90-37	+76.09	−239.83	+110.72	−1.05	−19.83	134.35	4	···	3
	G180-24	+113.43	−244.78	−19.96	−1.46	−24.78	115.17	4	···	3
	G232-18	+74.16	−241.16	+100.10	−1.01	−21.16	124.58	4	···	3
	HD105004[b]	−44.01	−240.07	−91.54	−1.09	−20.07	101.57	4	···	3
	HD233511	−128.43	−243.10	+32.62	−1.43	−23.10	132.51	4	···	3
	Wolf 610	+119.19	−246.19	+15.40	−1.17	−26.19	120.18	4	···	3
B3	−03 : 5166	+172.23	−297.98	+34.48	−1.51	−77.98	175.65	4	···	5
	−24 : 9840	+158.90	−292.48	−135.40	−1.69	−72.48	208.76	4	···	5
	877-025	+192.94	−303.31	−89.22	−1.14	−83.31	212.57	4	···	5
	G10-03	+187.91	−292.86	+84.93	−1.49	−72.86	206.21	4	···	5
	G15-24	−143.89	−259.35	+83.11	−1.35	−39.35	166.17	4	···	5
	G34-45	+184.25	−278.10	+46.66	−1.62	−58.10	190.07	4	···	5
	G89-14[b]	+202.53	−255.77	+19.87	−1.61	−35.77	203.50	4	···	5
	G98-53	−153.97	−261.45	−95.49	−1.09	−41.45	181.18	4	···	5
	HD3567	+167.42	−258.36	−49.12	−1.18	−38.36	174.48	4	···	5
B4	659-016	−34.63	−265.48	+43.74	−1.62	−45.48	55.79	4	7	···
	685-044*	+10.42	−275.01	+95.55	−1.41	−55.01	96.11	4	7	···
	G51-07	−41.62	−264.51	+24.26	−1.19	−44.51	48.17	4	7	···
	G53-41	−29.19	−295.60	−146.90	−1.22	−75.60	149.77	4	7	···
	G65-52[b]	−33.96	−275.99	−72.22	−1.33	−55.99	79.81	4	7	···
	G172-61[b]	−13.69	−262.52	+56.65	−1.11	−42.52	58.28	4	7	···
	HD106038	+25.71	−295.17	+18.91	−1.09	−75.17	31.92	4	7	···
	HD110621	−35.65	−262.26	+56.20	−1.56	−42.26	66.55	4	7	···
	LTT5864	−17.60	−280.57	−13.28	−1.51	−60.57	22.05	4	7	···
B5	808-022[b]	276.98	−261.48	−95.45	−1.20	−41.48	292.97	4	12	···
	G108-48	252.88	−287.42	−188.94	−1.15	−67.42	315.67	4	12	···
	G116-45	243.19	−242.67	+145.07	−1.08	−22.67	283.17	4	12	···
	G119-64	238.21	−290.86	−120.57	−1.49	−70.86	266.99	4	12	···
	G139-16*	259.56	−287.67	−51.63	−1.68	−67.67	264.64	4	12	···
	G154-25*	273.93	−263.08	−59.23	−1.43	−43.08	280.26	4	12	···
	G161-73*	258.45	−266.55	+38.77	−1.26	−46.55	261.34	4	12	···
B6	G03-22	+126.66	−164.30	+9.45	−0.45	55.70	127.01	12	···	4
	G13-38	+112.74	−140.17	+89.65	−0.77	79.83	144.04	12	···	4
	G29-20*	−66.30	−167.72	+95.50	−0.69	52.28	116.26	12	···	4
	G51-20	−22.13	−178.17	−80.95	−0.63	41.83	83.92	12	···	4
	G58-28	+36.43	−150.39	−63.87	−0.71	69.61	73.53	12	···	4
	G89-33	+33.58	−140.60	+96.74	−0.51	79.40	102.40	12	···	4
	G90-04	+69.34	−166.01	−29.33	−0.69	53.99	75.29	12	···	4
	G92-49*	−45.64	−150.95	−126.49	−0.54	69.05	134.47	12	···	4
	G99-02	+71.74	−182.62	+117.44	−0.66	37.38	137.62	12	···	4
	G128-36	+69.99	−135.51	−93.57	−0.41	84.49	116.85	12	···	4
	HD184499	−55.02	−147.22	+66.28	−0.69	72.78	86.14	12	···	4
	HIP54469	+98.18	−156.99	−89.70	−0.52	63.01	132.99	12	···	4

[b]Identified as a binary star by SIMBAD.
*From Table 1 or 2.

use the complete sample (i.e. including binaries) to define our final moving group candidates. Our entire sample of 1637 stars has been compared with members of each one of the Eggen groups looking for stars in common. From these shared stars, those belonging to any of our seven moving-group candidates have been identified. On the one hand, from this comparison, four of our moving-group candidates, namely G01-35, G18-24, G22-20, and G56-39, showed no stars in common with any of the groups of Eggen. On the other hand, there are four stars in common between our G03-37 group and

© Copyright 2012: Instituto de Astronomía, Universidad Nacional Autónoma de México

TABLE 12

FINAL MOVING GROUP CANDIDATES

Group	ID	U' [km s^{-1}]	V' [km s^{-1}]	W' [km s^{-1}]	[Fe/H] [dex]	$V_{\rm rot}$ [km s^{-1}]	$(U'^2+W'^2)^{1/2}$ [km s^{-1}]
G18-39	(A1+B3)						
	−03 : 5166	+172.23	−297.98	+34.48	−1.51	−77.98	175.65
	−24 : 9840	+158.90	−292.48	−135.40	−1.69	−72.48	208.76
	−48 : 2445	−217.17	−278.56	−10.50	−1.67	−58.56	217.42
	490-061	−198.54	−285.49	+24.15	−1.40	−65.49	200.00
	636-003[*,b]	+151.46	−255.97	−52.06	−1.55	−35.97	160.15
	709-053	−188.83	−288.69	+103.87	−1.48	−68.69	215.51
	877-025	+192.94	−303.31	−89.22	−1.14	−83.31	212.57
	G10-03	+187.91	−292.86	+84.93	−1.49	−72.86	206.21
	G15-24	−143.89	−259.35	+83.11	−1.35	−39.35	166.17
	G18-39	−190.57	−256.36	−17.39	−1.40	−36.36	191.36
	G31-26	−217.88	−304.88	+113.66	−1.37	−84.88	245.74
	G34-45	+184.25	−278.10	+46.66	−1.62	−58.10	190.07
	G36-47	−183.01	−274.73	−79.54	−1.49	−54.73	199.55
	G66-30[b]	−198.74	−271.86	+7.39	−1.57	−51.86	198.88
	G70-33	−207.69	−287.04	+61.44	−1.25	−67.04	216.59
	G86-39	−237.17	−278.35	−24.19	−1.44	−58.35	238.40
	G87-13	−198.27	−284.49	+15.80	−1.22	−64.49	198.90
	G89-14[b]	+202.53	−255.77	+19.87	−1.61	−35.77	203.50
	G98-53	−153.97	−261.45	−95.49	−1.09	−41.45	181.18
	G120-15	−239.44	−276.54	+12.81	−1.46	−56.54	239.78
	G157-85	−185.83	−288.49	−66.24	−1.35	−68.49	197.28
	G176-53	−228.07	−270.48	+60.61	−1.44	−50.48	235.99
	G187-30[b]	−227.66	−299.24	−34.54	−1.28	−79.24	230.27
	HD3567	+167.42	−258.36	−49.12	−1.18	−38.36	174.48
	HD101063[*]	−188.08	−250.90	+14.31	−1.30	−30.90	188.62
G21-22	(A2+B5)						
	808-022[b]	276.98	−261.48	−95.45	−1.20	−41.48	292.97
	G02-38[b]	219.81	−257.90	−53.68	−1.28	−37.90	226.27
	G21-22	249.46	−257.09	−29.61	−1.24	−37.09	251.21
	G82-42	212.29	−245.10	−136.78	−1.29	−25.10	252.54
	G108-48	252.88	−287.42	−188.94	−1.15	−67.42	315.67
	G116-45	243.19	−242.67	+145.07	−1.08	−22.67	283.17
	G119-64	238.21	−290.86	−120.57	−1.49	−70.86	266.99
	G139-16[*]	259.56	−287.67	−51.63	−1.68	−67.67	264.64
	G146-56	223.58	−263.03	+26.68	−1.32	−43.03	225.17
	G154-25[*]	273.93	−263.08	−59.23	−1.43	−43.08	280.26
	G161-73[*]	258.45	−266.55	+38.77	−1.26	−46.55	261.34
	HIP36878	212.66	−275.82	+90.99	−1.21	−55.82	231.31
G03-37	(A3+B4)						
	659-016	−34.63	−265.48	+43.74	−1.62	−45.48	55.79
	685-044[*]	+10.42	−275.01	+95.55	−1.41	−55.01	96.11
	G03-37	−54.45	−290.10	+37.76	−1.59	−70.10	66.26
	G05-36	−38.72	−292.97	−55.34	−1.20	−72.97	67.54
	G51-07	−41.62	−264.51	+24.26	−1.19	−44.51	48.17
	G53-41	−29.19	−295.60	−146.90	−1.22	−75.60	149.77
	G65-52[b]	−33.96	−275.99	−72.22	−1.33	−55.99	79.81
	G142-44	−46.48	−291.65	+63.09	−1.35	−71.65	78.36
	G170-56	−48.66	−288.86	−28.28	−1.11	−68.86	56.28
	G172-61[b]	−13.69	−262.52	+56.65	−1.11	−42.52	58.28
	G272-122	−43.54	−294.72	+32.70	−1.57	−74.72	54.45
	HIP22068	+0.58	−299.93	+81.28	−1.43	−79.93	81.28
	HIP59490	+25.71	−295.17	+18.91	−1.09	−75.17	31.92
	HIP62108	−35.65	−262.26	+56.20	−1.56	−42.26	66.55
	HIP69232	+46.92	−292.18	−1.75	−1.53	−72.18	46.95
	LTT5864	−17.60	−280.57	−13.28	−1.51	−60.57	22.05
G01-35	(A7+B6)						
	558-008	−64.69	−145.71	−41.49	−0.64	74.29	76.85
	G01-35	−119.32	−150.54	−14.45	−0.50	69.46	120.19
	G03-22	+126.66	−164.30	+9.45	−0.45	55.70	127.01
	G07-10	−88.21	−180.45	+96.04	−0.74	39.55	130.40
	G13-38	+112.74	−140.17	+89.65	−0.77	79.83	144.04
	G29-20[*]	−66.30	−167.72	+95.50	−0.69	52.28	116.26
	G51-20	−22.13	−178.17	−80.95	−0.63	41.83	83.92
	G57-07	−70.85	−160.65	−49.72	−0.54	59.35	86.56
	G58-28	+36.43	−150.39	−63.87	−0.71	69.61	73.53
	G89-33	+33.58	−140.60	+96.74	−0.51	79.40	102.40
	G90-04	+69.34	−166.01	−29.33	−0.69	53.99	75.29
	G92-49[*]	−45.64	−150.95	−126.49	−0.54	69.05	134.47
	G99-02	+71.74	−182.62	+117.44	−0.66	37.38	137.62
	G99-21	−60.97	−181.06	+23.69	−0.61	38.94	65.41
	G128-36	+69.99	−135.51	−93.57	−0.41	84.49	116.85
	HD184499	−55.02	−147.22	+66.28	−0.69	72.78	86.14
	HIP54469	+98.18	−156.99	−89.70	−0.52	63.01	132.99
G18-24	(A4)						
	G18-24[b]	−242.57	−209.15	−196.75	−1.49	10.85	312.33
	G179-54[b]	−301.04	−201.00	+87.39	−1.44	19.00	313.47
	G195-34	−269.12	−199.48	−20.68	−1.52	20.52	269.91
	G202-65[b]	−302.61	−215.51	−9.22	−1.41	4.49	302.75
G22-20	(A5)						
	G22-20	93.04	−213.17	+46.14	−1.01	+6.83	103.85
	G90-37	76.09	−239.83	+110.72	−1.05	−19.83	134.35
	G232-18	74.16	−241.16	+100.10	−1.01	−21.16	124.58
	HIP90261	44.87	−229.00	−102.25	−1.14	−9.00	111.66
G56-39	(A6)						
	G56-39	−90.96	−167.30	+4.09	−1.05	52.70	91.05
	G59-18[*]	−120.11	−173.94	−0.74	−1.20	46.06	120.11
	G83-26	−101.29	−148.57	+102.81	−1.19	71.43	144.32
	G269-87	−96.35	−152.24	−1.37	−1.13	67.76	96.36

[b]Identified as a binary star by SIMBAD. [*]From Table 1 or 2.

© Copyright 2012: Instituto de Astronomía, Universidad Nacional Autónoma de México

© Copyright 2012: Instituto de Astronomía, Universidad Nacional Autónoma de México

the *Kapteyn* group of Eggen (1990, 1996b,c) (and also four *Kapteyn* stars fall just outside the group A3+B4; see below). These groups share kinematic features like their low radial velocity, $\langle U' \rangle = -22$ and $\langle U' \rangle = +2$ km s^{-1} for G03-37 and *Kapteyn*, respectively. The G03-37 metallicity values approximate those of the *Kapteyn* group and considering the errors involved in photometric abundances at low metallicity ($\approx \pm 0.10$–0.25 dex), these metallicities agree quite well, in the range $-1.6 \lesssim$ [Fe/H] $\lesssim -1.3$. Finally, both have moderately retrograde movements in the Galaxy, $V_{\rm rot} \approx -65$ km s^{-1}. Thus, our G03-37 group is probably related to the *Kapteyn* group of Eggen.

In the case of the other two groups, G18-39 and G21-22, it is very interesting that their negative V' values indicate a slightly retrograde movement in the Galaxy, and their average metallicities and rotational velocities resemble those of the ω Cen group identified by Meza et al. (2005). Since they have restricted the ω Cen group members to thirteen stars with $-600 < J_z < +300$ km s^{-1} kpc and orbits close to the Galactic disk with $|W| < 65$ km s^{-1}, we were not able to identify individual stars in common with these two groups, and so a kinematical and chemical-abundance comparison has been made based on the typical photometric [Fe/H]s of these halo field stars plus their Galactic velocities as derived here.

Meza et al. (2005) (see also Dinescu 2002; Bekki & Freeman 2003; Tsuchiya, Korchagin, & Dinescu 2004) investigate the orbital characteristics of tidal debris from satellites on eccentric orbits, coplanar with the disk, having a gravitational encounter with our Galaxy. Their numerical simulations showed that this kind of interaction is expected to strip stars from the original satellite and leave them in 'trails' of different orbital energy and angular momentum. These stars would show to an observer, located in between the apocenter and pericenter of their orbits, as different groups of stars with low vertical velocity and a broad, symmetric, and often double-peaked radial-velocity (U') distribution (Meza et al. 2005, their Figure 7). These kinematical characteristics are present in our G18-39 and G21-22 groups; see Figure 7, where concentrations of halo stars are seen at $U' \approx -200$ and $U' \approx +225$. The rotational velocity of the ω Cen group members, as identified by Meza et al. (2005, their Figure 8), lies in the range $-50 < V_{\rm rot} < 0$ km s^{-1} while our group velocities range between -85 km s^{-1} and -20 km s^{-1} for G18-39 and G21-22. The wide ranges in the U' velocity are very similar, $-300 < U' < +300$ km s^{-1} for the ω Cen group, as identified by Meza et al. (2005), and $-250 < U' < +275$ km s^{-1} for G18-39 and G21-22. Their simulations (Meza et al. 2005, their Figure 7) show "double-humps" in U' at about ± 175 km s^{-1} for R $\approx$8.5 kpc, while G18-39 and G21-22 show peaks at about -200 and $+225$ km s^{-1}, Figure 7. Finally, the metallicity range of the ω Cen group and our groups are very similar, actually overlapping, $-2.6 <$ [Fe/H] < -0.9 and $-1.69 <$ [Fe/H] < -1.08 (Table 12), respectively. More recently, the high-resolution spectroscopic work of Johnson & Pilachowski (2010) find a metallicity range of $-2.2 \lesssim$ [Fe/H] $\lesssim -0.6$ for individual stellar members of ω Cen with four peaks in the [Fe/H] histogram, occurring at [Fe/H] ≈ -1.75, -1.5, -1.15, and -0.75. The G18-39 and G21-22 groups have mean photometric metallicities of $\langle$ [Fe/H] $\rangle \approx -1.41$ and -1.30, respectively.

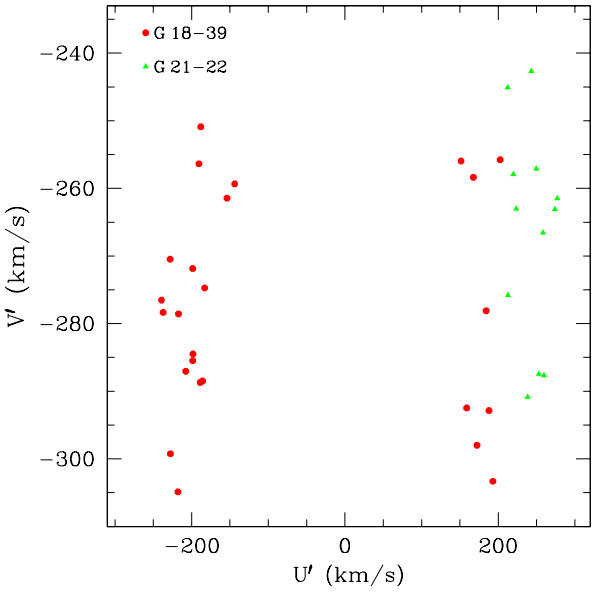

Fig. 7. Bottlinger diagram for two of the moving groups discussed in the text, where it can be appreciated the double structure in the velocity U' as forecast by the models of Meza et al. (2005) for the accretion by the Milky Way of a dwarf galaxy similar to the probable progenitor of ω Cen.

Thus, it is quite possible that the dynamical and chemical characteristics of our halo Groups G18-39 and G21-22 are compatible with the simulations of Meza et al. (2005). This suggests that these two candidate groups are related to the ω Cen stream, or at least to some similar dwarf galaxy accreted by the Galaxy, but whose stars were captured by the Galaxy not quite as close to the Galactic plane as in these simulations, and with slightly higher radial energies.

© Copyright 2012: Instituto de Astronomía, Universidad Nacional Autónoma de México

Recently, Wylie-de Boer et al. (2010) suggest the presence of tidal debris from the ω Cen progenitor in the *Kapteyn* group, based on kinematic and high-resolution spectroscopic analysis of 16 members of this group. They suggest that at least 14 members of the *Kapteyn* group, but maybe more, could be debris remnants from the progenitor dwarf galaxy of ω Cen. The abundances of [Na/Fe], [Mg/Fe], [Zr/Fe], and [Ba/Fe] show great similarity between the Kapteyn and ω Cen stars, but both these groups are dissimilar to general halo field stars (comparisons of the abundance of [Ca/Fe] are inconclusive). There is only one star (HIP 62108) in common between their list of 14 Kapteyn stars and our group G03-37, but four other of their Kapteyn stars (G24-03, G18-54, HD 181743, and HD 215801) lie just outside our A3 and B4 groupings, as defined above. These results would also indicate that our G03-37 group, originally related to Eggen's Kapteyn group, is also related to the ω Cen stream, and that perhaps evidence for the remnants of ω Cen is ubiquitous in the solar neighborhood, especially within stars with moderately retrograde orbits, $-100 \lesssim V_{\rm rot} \lesssim -20$ (see the 'low-alpha' halo stars of Nissen & Schuster (2010, 2011); Schuster et al. (2012), from the solar neighborhood, and their possible connection to ω Cen; also the results by Dinescu (2002). This G03-37 moving group does not contribute to the double-peaked radial-velocity structure of Meza et al. (2005), as do G18-39 and G21-22, but rather to the structure of the broad intervening velocity distribution of this simulation (Meza et al. 2005, their Figure 7). Also, the mean [Fe/H], V', and W' values for the stars of this G03-37 group do not disagree with those values suggested above for the ω Cen stream.

7. CONCLUSIONS

The main conclusions of this work are the following:

1. Two photometric catalogues of standard $uvby-\beta$ data are presented here for metal-poor stars selected from the literature to have [Fe/H] $\lesssim -2.0$, and for metal-poor subgiant candidates. These data are on the same-quality photometric system as our previous $uvby-\beta$ catalogues (Schuster & Nissen 1988; Schuster et al. 1993, 2006).

2. It can be seen in the $(b-y)_0, c_0$ diagram of Figure 2 and in Tables 3 and 4 that a number of these stars have been mis-classified either as to their low metallicity or to their being subgiants. In Figure 2 a number of the supposed "subgiants" appear more as main-sequence stars; this may indicate an actual previous spectroscopic or photometric mis-classification, or to a present photometric mis-classification due to anomalous abundances of C and/or N and their effects upon the Strömgren indices, as discussed in the text for the CH giant G24-25. In Table 3 many of the metal-poor stars have metallicities significantly above [Fe/H] ≈ -2.0 with a considerable number having even [Fe/H] > -1.0; this again may indicate previous errors of abundance measurement, or the photometric effects of anomalous abundances of other elements with respect to iron. These stars represent interesting candidates for further spectroscopic study.

3. By examining stellar density contours in the [Fe/H] vs $V_{\rm rot}$, Bottlinger (V' vs U'), and Toomre (V' vs $(U'^2+W'^2)^{1/2}$) diagrams, a number of moving-group candidates have been identified for the Galactic halo. Some of these, our "A" groups, have four or more overlapping stellar members in all three of these diagrams, while others, the "B" groups, have four or more overlapping members in only two of these diagrams. Some of these "A" and "B" groups have been combined to give the seven best moving-group candidates, shown in Table 12: G18-39 (A1+B3; 25 possible members), G21-22 (A2+B5; 12), G03-37 (A3+B4; 16), G01-35 (A7+B6; 17), G18-24 (A4; 4), G22-20 (A5; 4), and G56-39 (A6, 4).

4. Two of our moving-group candidates, G18-39 and G21-22, provide a double-peaked structure in the U'-velocity distribution for moderately retrograde halo stars (Figure 7), very similar to that structure produced in the simulations by Meza et al. (2005) for the accretion by the Milky Way of a dwarf galaxy similar to the probable progenitor of ω Cen. This result ties in closely with many other results in the literature suggesting a significant contribution of tidal remnants from ω Cen in the solar neighborhood.

5. Four of our members from the G03-37 moving-group candidate are found in the lists of members of the Kapteyn moving group proposed by Eggen (1990, 1996b,c), and four other stars from these lists by Eggen fall just outside our groupings A3 and B4, defined in Tables 10–11 as drawn from our Figures 3–6. It seems most probable then that our G03-37 moving-group

© Copyright 2012: Instituto de Astronomía, Universidad Nacional Autónoma de México

candidate relates closely to this classic moving group by Eggen (1990, 1996b,c).

6. One of our stars from G03-37, plus the four stars near the groupings A3+B4, mentioned above, have also been connected to possible remnants of ω Cen by the high-resolution chemical and detailed dynamical analyses of Wylie-de Boer et al. (2010) for 16 members of the Kapteyn moving group. So, it seems evident that this third moving group of the present work is also related to ω Cen, emphasizing again the omnipresence of evidence for remnants of ω Cen in the solar neighborhood, especially amongst halo stars with moderately retrograde orbits, $-100 \lesssim V_{\rm rot} \lesssim -20$.

7. Most of the moving-group candidates identified in this present work, Table 12: G18-39, G21-22, G01-35, G18-24, G22-20, and G56-39, are new and not found in the literature, providing ample opportunity for new high-resolution spectroscopic and detailed dynamical studies. The groupings B1 and B2, which have not received much attention in this work and which show the overlap of 6–7 stars between the [Fe/H] vs $V_{\rm rot}$ and Toomre diagrams, also provide possibilities for further studies; in fact, these two groupings also show similarities in [Fe/H], $V_{\rm rot}$, and possibly U' to probable remnants from ω Cen.

This work was supported by the Conacyt projects CB-2005-01-49434 and CB-2005-49002, and we are very appreciative of this funding which helped considerably with the data reductions and analyses. We thank very much the support and technical staff at the San Pedro Mártir Observatory for their considerable help during the taking of the $uvby-\beta$ photometric data. As always, B. Hernández has helped expertly with the computer systems and software. We also thank Sean Ryan and Bruce Carney for sharing their lists of metal-poor and subgiant stars.

REFERENCES

Abadi, M. G., Navarro, J. F., Steinmetz, M., & Eke, V. R. 2003a, ApJ, 591, 499
_____. 2003b, ApJ, 597, 21
Abt, H. A., & Biggs, E. S. 1972, Bibliography of Stellar Radial Velocities (New York: Latham Process Corp.)
Antoja, T., Figueras, F., Fernández, D., & Torra, J. 2008, A&A, 490, 135
Antoja, T., Figueras, F., Romero-Gómez, M., Pichardo, B., Valenzuela, O., & Moreno, E. 2011, MNRAS, 418, 1423
Antoja, T., Figueras, F., Torra, J., Valenzuela, O., & Pichardo, B. 2010, Lecture Notes Essays Astrophys. IV, 4, 13
Antoja, T., Valenzuela, O., Pichardo, B., Moreno, E., Figueras, F., & Fernández, D. 2009, ApJ, 700, L78
Asiain, R., Figueras, F., Torra, J., & Chen, B. 1999, A&A, 341, 427
Barbier-Brossat, M., & Figon, P. 2000, A&AS, 142, 217
Barbier-Brossat, M., Petit, M., & Figon, P. 1994, A&AS, 108, 603
Barrado y Navascués, D. 1998, A&A, 339, 831
Bekki, K., & Freeman, K. C. 2003, MNRAS, 346, L11
Carney, B. W., Latham, D. W., Laird, J. B., & Aguilar, L. A. 1994, AJ, 107, 2240
Chereul, E., Crézé, M., & Bienaymé, O. 1998, A&A, 340, 384
Correnti, M., Bellazzini, M., Ibata, R. A., Ferraro, F. R., & Varghese, A. 2010, ApJ, 721, 329
Crawford, D. L. 1975, AJ, 80, 955
Crawford, D. L., & Barnes, J. V. 1970, AJ, 75, 978
Crawford, D. L., & Mander, J. 1966, AJ, 71, 114
Dehnen, W. 1998, AJ, 115, 2384
_____. 2000, AJ, 119, 800
Dinescu, D. I. 2002, in ASP Conf. Ser. 265, Omega Centauri, A Unique Window into Astrophysics, ed. F. van Leeuwen, J. D. Hughes, & G. Piotto (San Francisco: ASP), 365
Eggen, O. J. 1958, MNRAS, 118, 65
_____. 1960a, MNRAS, 120, 540
_____. 1960b, MNRAS, 120, 563
_____. 1965, in Galactic Structure, Vol. 5 of Stars and Stellar Systems, Chapter 6, Moving Groups of Stars, ed. A Blaauw & M. Schimdt (Chicago: Univ. Chicago Press), 111
_____. 1971, PASP, 83, 271
_____. 1975, PASP, 87, 37
_____. 1977, ApJ, 215, 812
_____. 1983a, AJ, 88, 642
_____. 1983b, AJ, 88, 813
_____. 1983c, MNRAS, 204, 377
_____. 1983d, MNRAS, 204, 391
_____. 1984, AJ, 89, 1358
_____. 1990, AJ, 100, 1159
_____. 1991, AJ, 102, 2028
_____. 1992a, AJ, 103, 1302
_____. 1992b, AJ, 104, 1482
_____. 1992c, AJ, 104, 1493
_____. 1994, in Galactic and Solar System Optical Astrometry, ed. L. V. Morrison & G. Gilmore (Cambridge: Cambridge Univ. Press), 191
_____. 1995a,AJ, 110, 1749
_____. 1995b, AJ, 110, 2862
_____. 1996a, AJ, 111, 1615
_____. 1996b, AJ, 112, 1595
_____. 1996c, AJ, 112, 2661
_____. 1998a, AJ, 116, 284
_____. 1998b, AJ, 116, 782
Eggen, O. J., Lynden-Bell, D., & Sandage, A. R. 1962, ApJ, 136, 748 (ELS)
Eggen, O. J., & Sandage, A. R. 1959, MNRAS, 119, 255
ESA 1997, The Hipparcos and Tycho Catalogues ESA SP-1200 (Noordwijk: ESA)
Famaey, B., Jorissen, A., Luri, X., Mayor, M., Udry, S., Dejonghe, H., & Turon, C. 2005, A&A, 430, 165

Famaey, B., Siebert, A., & Minchev, I. 2011, arXiv:1110.6176
Fouts, G., & Sandage, A. 1986, AJ, 91, 1189
Freeman, K., & Bland-Hawthorn, J. 2002, ARA&A, 40, 487
Fux, R. 2001, A&A, 373, 511
Giclas, H. L., Burnham, R., Jr., & Thomas, N. G. 1961, Lowell Obs. Bull., 5, 61
_____. 1975, Lowell Obs. Bull., 8, 9
Giclas, H. L., Slaughter, C. D., & Burnham, R., Jr. 1959, Lowell Obs. Bull., 4, 136
Goldberg, D., Mazeh, T., Latham, D., Stefanik, R., Carney, B., & Laird, J. 2002, AJ, 124, 1132
Grønbech, B., Olsen, E. H., & Strömgren, B. 1976, A&AS, 26, 155
Grundahl, F., VandenBerg, D. A., Stetson, P. B., Andersen, M. I., & Briley, M. 2000, in The Galactic Halo: From Globular Clusters to Field Stars, ed. A. Noels et al. (Liège: Inst. d'Astrophys. et Geophys.), 503
Helmi, A., Navarro, J. F., Nordström, B., Holmberg, J., Abadi, M. G., & Steinmetz, M. 2006, MNRAS, 365, 1309
Hertzsprung, E. 1909, ApJ, 30, 135
Høg, E., et al. 2000, A&A, 355, L27
Johnson, C. I., & Pilachowski, C. A. 2010, ApJ, 722, 1373
Johnson, R. H., & Soderblom, D. R. 1987, AJ, 93, 864
Kalnajs, A .J. 1991, in Dynamics of Disks Galaxies, ed. B. Sundelius (Göteborgs: Göteborgs Univ. & Chalmers Univ. of Technology), 323
Kapteyn, J. C. 1905, Reports British Assoc. Advancement of Science, 264, 257
Keller, S. C., Da Costa, G. S., & Prior, S. L. 2009, MNRAS, 394, 1045
Klement, R., et al. 2009, ApJ, 698, 865
Latham, D. W., Mazeh, T., Carney, B., McCrosky, R., Stefanik, R., & Davis, R. 1988, AJ, 96, 567
Latham, D. W., et al.1992, AJ, 104, 774
Latham, D. W., et al.2002, AJ, 124, 1144
Lindblad, B. 1925, ApJ, 62, 191
Liu, S., Nissen, P. E., Schuster, W. J., Zhao, G., Chen, Y. Q., & Liang, Y. C. 2011, A&A, submitted
Luyten, W. J. 1979a, NLTT Catalog of Stars with Proper Motions Larger than Two Tenths of an Arcsecond (Minneapolis: Univ. of Minnesota Press)
_____. 1979b, LHS Catalogue. A Catalogue of Stars with Proper Motions Exceeding 0″5 Annually (2nd ed.; Minneapolis: Univ. of Minnesota Press)
Majewski, S. R., Ostheimer, J. C., Kunkel, W. E., & Patterson, R. J. 2000, AJ, 120, 2550
Mayor, M. 1972, A&A, 18, 97
Meléndez, J., Schuster, W. J., Silva, J. S., Ramírez, I., Casagrande, L., & Coelho, P. 2010, A&A, 522, A98
Meza, A., Navarro, J. F., Abadi, M. G., & Steinmetz, M. 2005, MNRAS, 359, 93
Montes, D., López-Santiago, J., Gálvez, M. C., Fernández-Figueroa, M. J., De Castro, E., & Cornide, M. 2001, MNRAS, 328, 45
Morrison, H. L., et al.2000, AJ, 119, 2254
Muñoz, R. R., et al.2006, ApJ, 649, 201
Navarro, J. F., Helmi, A., & Freeman, K. C.2004, ApJ, 601, L43
Nissen, P. E., & Schuster, W. J. 1991, A&A, 251, 457
_____. 2010, A&A, 511, L10
_____. 2011, A&A, 530, A15
Nordström, B., et al. 2004, A&A, 418, 989
Olsen, E. H. 1983, A&AS, 54, 55
_____. 1984, A&AS, 57, 443
Prior, S. L., Da Costa, G. S., & Keller, S. C. 2009, ApJ, 704, 1327
Proctor, R. A. 1869, R. 1995, Proc. Roy. Soc. London, 18, 169
Quinn, P. J., & Goodman, J. 1986, ApJ, 309, 472
Rocha-Pinto, H. J., Majewski, S. R., Skrutskie, M. F., & Crane, J. D. 2003, ApJ, 594, L115
Röser, S., & Bastian, U. 1991, PPM Star Catalogue by the Astronomisches Rechen-Institut Heidelberg (Heidelberg: Spektrum Akademischer Verlag)
Ryan, S. G., & Norris, J. E. 1991, AJ, 101, 1835
Salim, S., & Gould, A. 2003, ApJ, 582, 1011
Schuster, W. J., & Nissen, P. E. 1988, A&AS, 73, 225
_____. 1989, A&A, 221, 65
Schuster, W. J., Beers, T. C., Michel, R., Nissen, P. E., & García, G. 2004, A&A, 422, 527
Schuster, W. J., Moitinho, A., Márquez, A., Parrao, L., & Covarrubias, E. 2006, A&A, 445, 939
Schuster, W. J., Moreno, E., Nissen, P. E, & Pichardo, B. 2012, A&A, 538, A21
Schuster, W. J., Parrao, L., & Contreras, M. E. 1993, A&AS, 97, 951
Searle, L., & Zinn, R. 1978, ApJ, 225, 357 (SZ)
Sharma, S., Johnston, K. V., Majewski, S. R., Muñoz, R. R., Carlberg, J. K., & Bullock, J. 2010, ApJ, 722, 750
Skuljan, J., Hearnshaw, J. B., & Cottrell, P. L. 1999, MNRAS, 308, 731
Soderblom, D. R., & Mayor, M. 1993a, AJ, 105, 226
_____. 1993b, ApJ, 402, L5
Starkenburg, E., et al. 2009, ApJ, 698, 567
Tsuchiya, T., Korchagin, V. I., & Dinescu, D. I. 2004, MNRAS, 350, 1141
Vivas, A. K., Jaffé, Y. L., Zinn, R., Winnick, R., Duffau, S., & Mateu, C. 2008, AJ, 136, 1645
Wylie-de Boer, E., Freeman, K., & Williams, M. 2010, AJ, 139, 636
Wyse, R. F. G., et al. 2006, ApJ, 639, L13
Začs, L., Nissen, P. E., & Schuster, W. J. 1998, A&A, 337, 216
Zinn, R., Vivas, A. K., Gallart, C., & Winnick, R. 2004, in ASP Conf. Ser. 327, Satellite and Tidal Streams, ed. F. Prada, D. Martínez-Delgado, & T. Mahoney (San Francisco: ASP), 92

J. S. Silva: Observatório Nacional/MCT. Rua Gal. José Cristino 77, São Cristóvão, CEP20291-400 Rio de Janeiro RJ, Brazil (jsergio@on.br).
M. E. Contreras, W. J. Schuster, and J. S. Silva: Instituto de Astronomía, Universidad Nacional Autónoma de México, Apdo. Postal 877, 22800 Ensenada, B.C., Mexico (mcontreras, schuster, jsilva@astrosen.unam.mx).

© Copyright 2012: Instituto de Astronomía, Universidad Nacional Autónoma de México